ADVANCED MATERIALS
www.advmat.de

# Perovskites for Light Emission

*Li Na Quan, F. Pelayo García de Arquer, Randy P. Sabatini, and Edward H. Sargent**

**Next-generation displays require efficient light sources that combine high brightness, color purity, stability, compatibility with flexible substrates, and transparency. Metal halide perovskites are a promising platform for these applications, especially in light of their excellent charge transport and bandgap tunability. Low-dimensional perovskites, which possess perovskite domains spatially confined at the nanoscale, have further extended the degree of tunability and functionality of this materials platform. Herein, the advances in perovskite materials for light-emission applications are reviewed. Connections among materials properties, photophysical and electrooptic spectroscopic properties, and device performance are established. It is discussed how incompletely solved problems in these materials can be tackled, including the need for increased stability, efficient blue emission, and efficient infrared emission. In conclusion, an outlook on the technologies that can be realized using this material platform is presented.**

## 1. Introduction

Metal halide perovskites (MHPs) have recently been established as an important class of materials that exhibit promising magnetic, electrical, and optical properties.[1,2] The chemical and structural diversity of this materials' family enables a large range of optoelectronic applications.[3] This class of materials combines solution processing with materials' properties that in cases can approach the quality of highly crystalline industry reference materials such as GaAs and Si.

In MHP photovoltaics (PV), power conversion efficiencies (PCEs) have increased to 22.7% over a 5 year period of intensive research.[4–9] These outstanding properties for PV applications translate into compelling properties for light-emitting applications.[10] MHPs have been proven to be good light emitters, and early on attracted attention for their potential in light-emitting diodes (LEDs) and lasers.[11–13] By engineering perovskites' chemical composition and structure, researchers have increased the photoluminescence (PL) efficiency of perovskite solids to near unity.[14] In the past 3 years, perovskite LED efficiency has increased in external quantum efficiency (EQE) from 0.0125% to greater than 10%.[15,16] The devices exhibit promising color purity, high luminance, and high mobility. Challenges remain in the form of 1) the need for further increases in device efficiency to meet and surpass organic LEDs (OLEDs) and inorganic quantum dot LEDs[17] and 2) the need for dramatic progress in device stability.

MHP LEDs consist of an intrinsic light-emission active layer in a double-heterojunction structure with an n-type electron injection layer (EIL) and a p-type hole-injection layer (HIL) (**Scheme 1**). Charge carriers are injected into a luminescent layer under forward bias, where they recombine radiatively. Early demonstrations of MHP LEDs date back to 1990[18] with 2D layered perovskites. In 2014, room-temperature (RT) perovskite LEDs used $MAPbI_{3-x}Cl_x$, $MAPbI_{3-x}Br_x$, and $MAPbBr_3$ as the emitting layer for near-infrared, red, and green, respectively.[11,15] The maximum EQE for perovskite LEDs has recently reached 12% in the near-infrared and 14% in the green.[16,19]

Here, we address the potential of optically and electrically excited perovskites of different types to meet the requirements of high color quality lighting and display technologies. We discuss the key advantages of using perovskites as luminophores for light-emitting applications and outline the challenge from a materials science's perspective. We examine the different types of perovskite light-emitting materials as well as fundamental photophysical and distinctive optical properties. We discuss also device architectures in perovskite LEDs and interface engineering strategies. We conclude by presenting recent advances and promising directions to overcome the low stability of perovskites—their current chief challenge for light-emitting applications.

## 2. Perovskite Fundamentals

In this section, we present the main classes of metal halide perovskites and their properties as a function of dimensionality.

### 2.1. Hybrid Perovskites

Perovskite refers to a large family of crystalline ceramics with 3D structures based on that of the natural mineral calcium titanium oxide. The mineral was discovered in the Ural Mountains of Russia by Gustav Rose in the 1800s and is named after Russian mineralogist Lev Perovski.[20] The general chemical formula of the perovskites is $AMX_3$, where "X" as an anion bonding with "A" and "M" cations with different sizes (**Figure 1**).[21] Here the 3D network is made of a series of corner-sharing $MX_6$ octahedra with the "A" cations occupying

Dr. L. N. Quan, Dr. F. P. G. de Arquer, Dr. R. P. Sabatini, Prof. E. H. Sargent
Department of Electrical and Computer Engineering
University of Toronto
10 King's College Road, Toronto, Ontario M5S 3G4, Canada
E-mail: ted.sargent@utoronto.ca

DOI: 10.1002/adma.201801996

 

the cubo-octahedral cavities, maintaining electroneutrality of the system. Treating all ions as rigid spheres and considering a close packing configuration yields the Goldschmidt's tolerance factor concept, namely $(R_A + R_X) = t\sqrt{2}(R_B + R_X)$, where $t$ is the tolerance factor and $R_A$, $R_B$, and $R_X$ are ionic radii for the corresponding ions.[22] The tolerance factor for ionic radii is useful for predicting new perovskite structures. Typical 3D perovskites have tolerance factors between $0.8 \leq t \leq 1.0$.[23]

In the case of MHPs, the A-site is occupied by a small organic cation (e.g., $CH_3NH_3^+$ and $CH_3(NH_2)^{2+}$), while M-site is a divalent metal (e.g., $Pb^{2+}$, $Sn^{2+}$, or $Ge^{2+}$) and the X-site is a halogen (e.g., $I^-$, $Br^-$, or $Cl^-$). The bandgap of MHPs can be tuned by varying the combination of all three cationic and anionic components.[24] Varying the "A" cation causes changes in the "M—X" bond which ultimately expands and contracts the perovskite lattice. Typical "A" cations such as $Cs^+$, methylammonium ($MA^+$), or formamidinium ($FA^+$) can form a 3D framework with the $PbI_6$ network, where the effective ionic radius ($R$) follows a trend of $R_{Cs+} < R_{MA+} < R_{FA+}$. An increase in the ionic radius of the "A" cation leads to an overall lattice expansion, which also correlates with a decrease of the bandgap of the MHPs.[25]

In the MHP family, "M" is a divalent metal cation such as $Pb^{2+}$, $Sn^{2+}$, $Cu^{2+}$, $Ni^{2+}$, $Co^{2+}$, or $Mn^{2+}$, and the differences in "X—M—X" bond angle impact the tuning of the bandgap.[26] Pb-based MHPs produce a bathochromic shift in the absorption spectra when the size of the "X" halogen is increased. This is due to the increase in covalent character of the electronegativity of the halogen atom. Hence, optical absorption can be easily tuned by bandgap engineering of MHPs across the visible spectrum.[27]

Facile tuning of the bandgap in MHPs across the visible and near-infrared (NIR) spectrum increases their interest in light-emitting applications including LEDs and lasers. Their excellent charge transport properties and large mobilities entail, however, another challenge: a low probability of radiative recombination which means that they require high excitation fluences to attain high photoluminescence quantum yield (PLQY) and bright emission.

Low-dimensional perovskites (2D perovskites and perovskite nanocrystals (NCs)) have recently been introduced that address this limitation and also introduce an additional lever to tune light emission.

### 2.2. Low-Dimensional Perovskites

Low-dimensional MHPs are a subclass of perovskites truncated and confined along at least one axis. 2D MHPs consist of sheets of perovskite unit cells: periodic along a basal plane and confined in the perpendicular direction. This can be pictured as the 3D $AMX_3$ perovskite cut into one repeat unit thick slices along the ⟨100⟩ direction, where A and X ions within the slice planes are cut into halves.[28] The monolayer inorganic perovskite slabs are typically sandwiched between organic amine molecules, and the corresponding 2D perovskite is produced after substitution by the appropriate organic molecules, which can be expressed by $(R—NH_3)_2MX_4$. $R—NH^{3+}$ is an aliphatic or aromatic ammonium cation, where the M cation is generally a divalent metal that can adopt an octahedral anion coordination, such as Pb, Sn, Cu, or Ge,[29] and X is a halogen.

**Li Na Quan** received her Ph.D. from Ewha Womans University (2016) under the supervision of Prof. Dong Ha Kim. She worked at the University of Toronto during 2014 to 2016 as a visiting graduate student and a postdoctoral researcher from 2016 to 2017, under the supervision of Prof. Edward. H. Sargent. She currently works as a postdoctoral researcher at the University of California, Berkeley in the group of Prof. Peidong Yang. Her research focuses on layered perovskites for light emission and photovoltaic applications and photophysical studies.

**F. Pelayo García de Arquer** pursued Telecommunications B.Sc. and M.Sc. studies at Universidad de Oviedo and Mathematical Sciences studies at UNED. After an M.Sc. in photonics at UPC Barcelona Tech., he carried out his Ph.D. at the Institute of Photonic Sciences (ICFO), where he focused on the application of novel plasmoelectric phenomena to optoelectronic devices such as photodetectors and solar cells. He is now a postdoctoral research fellow at the University of Toronto in the Sargent group. His current research interests include the use of functional nanomaterials for energy harvesting and storage applications.

**Edward H. Sargent** holds the rank of University Professor and Canada Research Chair in Nanotechnology at the University of Toronto. He received his B.Sc. Eng. (engineering physics) from Queen's University in 1995 and Ph.D. in electrical and computer engineering (photonics) from the University of Toronto in 1998. He has been Visiting Professor at MIT, UCLA, and Berkeley. He was founder and CTO of InVisage Technologies.

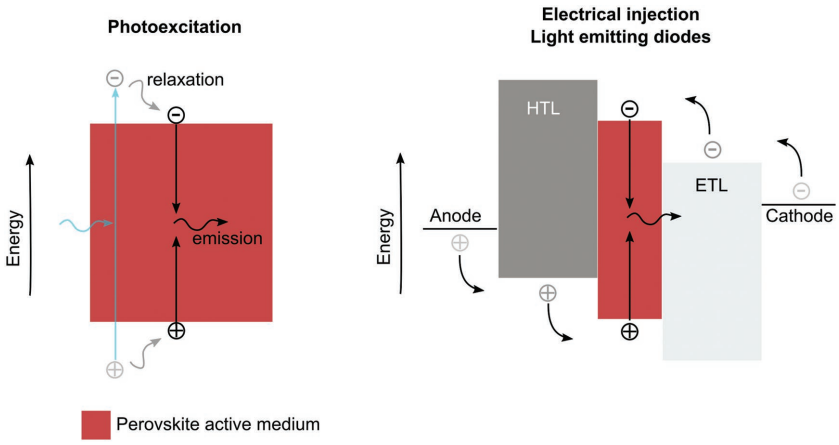


**Scheme 1.** Photo and electrical excitation of perovskite materials.

2D perovskites are analogous to the Ruddlesden–Popper phase of $K_2NiF_4$ material. Mitzi et al. pioneered layered perovskites in the 1990s introducing $(C_4H_9NH_3)_2(CH_3NH_2)_{n-1}Sn_nI_{3n+1}$. The crystal structure of 2D perovskites can be modified by altering the combination of organic and inorganic salts, tailoring thereby the electronic, optical, and magnetic properties.[30] 2D MHPs exhibit a quantum well energy landscape, where the inorganic $(MX_4)^{2-}$ structure acts as a quantum well and the organic $(R{-}NH_3)^{2+}$ capping layers as a quantum barrier. The highest occupied molecular orbital (HOMO)–lowest unoccupied molecular orbital (LUMO) bandgap of the organic layers is higher than the bandgap of the inorganic layers,[31] which leads to an enhancement of electron–hole Coulomb interaction. Confinement leads to a strongly bound excitons, up to 300–400 meV for phenylethylammonium (PEA) lead iodide $((C_6H_4CH_2CH_4NH_3)_2PbI_4)$ MHP, at room temperature (RT).[32] The large exciton binding energy and oscillator strength also lead to strong PL, nonlinear optical effects, and tunable polariton absorption.[33]

In addition to a single-layer perovskite sheet, these structures can also be conveniently synthesized with multiple ⟨100⟩-oriented sheets, enabling control over the dimensionality of the inorganic framework of the 3D perovskite structures. When one finetunes the proportions between the two organic ligands, one may synthesize inorganic sheets of different dimensions.[34]

The higher formation energy of low-dimensional perovskites endows them with an increased moisture stability.[35,36] In sum, layered perovskites are a promising subclass of MHPs with favorable electronic properties for light-emission applications.[37]

### 2.3. Perovskite Nanocrystals

Inorganic 0D perovskite-based colloidal $CsPbX_3$ (X = Cl, Br, and I) NCs are another class of perovskites with attractive properties for light emission. These inorganic perovskite nanocrystals are typically synthesized by reaction between cesium carbonate and oleic acid in a solution of metal halides. Kovalenko and co-workers first fabricated the $CsPbX_3$ structure with exceptionally tunable optical properties and high PLQY.[38] In light of the increased exciton binding energy in small-sized NCs, the PL emission is more likely to originate from exciton recombination rather than from bimolecular recombination of free carriers.[39]

0D perovskites present a spectral range spanning from 400 to 700 nm through both halide composition and quantum tuning, suggesting a major opportunity to employ this family of materials for light-emission applications in the visible.[38,40–42]

$CsPbX_3$ perovskite NCs show impressively efficient and narrower PL, as well finer size tuning of emission peaks, compared to conventional rare-earth phosphors, organic polymers, and dyes. $CsPbX_3$ NCs allow for a wider gamut of pure colors than the current high definition standard (Commision Internationale de l'Eclairage (CIE) chromaticity diagram). Perovskite NCs have also been of great interest as emissive materials in phosphor-converted white LEDs with GaN blue chips.[43]

Today, the formation of thin-film based on $CsPbX_3$ perovskite NCs still needs further improvement; at present, reliance on hydrophobic insulating long ligands hinders stability and processability.[44]

## 3. Photophysics of Perovskite Light Emission

The photophysical cycle (**Figure 2**) begins with the introduction of electrons and holes in the conduction and the valence band, respectively, via either an optical or an electrical source. From this point, competition occurs between different radiative and nonradiative pathways, and the specific photophysical route is strongly influenced by the perovskite dimensionality and structure (**Table 1**).[45,46]

For photoexcitation, 3D $CH_3NH_3PbI_3$ perovskite was observed to have an absorption coefficient ranging from $5 \times 10^3$ to $5 \times 10^4$ $cm^{-1}$ throughout the visible region, roughly one order of magnitude higher than that observed for conventional ruthenium-based dyes.[47] This helped move perovskites quickly to the upper reaches of the photovoltaic efficiency chart for solution-processed materials.[48] Nonlinear absorption has also been reported: two-photon absorption has been demonstrated for 3D films,[49] 3D single crystals,[50] 2D flakes,[51] and nanocrystals,[52,53] with coefficients up to 211 cm $MW^{-1}$.[51] Even five-photon absorption has been reported in the case of core–shell perovskite nanocrystals.[54]

While MHPs exhibit efficient light absorption, the exact nature of the resulting excited state (exciton vs free charge carrier) has long been under debate. For iodine-based 3D perovskites, the reported exciton binding energy has ranged from 50[55] to 2 meV.[56] Today, values in the lower range are the most accepted.[57] Given that $kT$ is ≈25 meV at room temperature, these suggest that the excited state is composed mostly of carriers. Indeed, time-resolved photoluminescence and transient absorption spectroscopy have shown that the optical responses of iodine-based 3D perovskites are dominated by free carriers.[58–61] The behavior of charge carriers was further

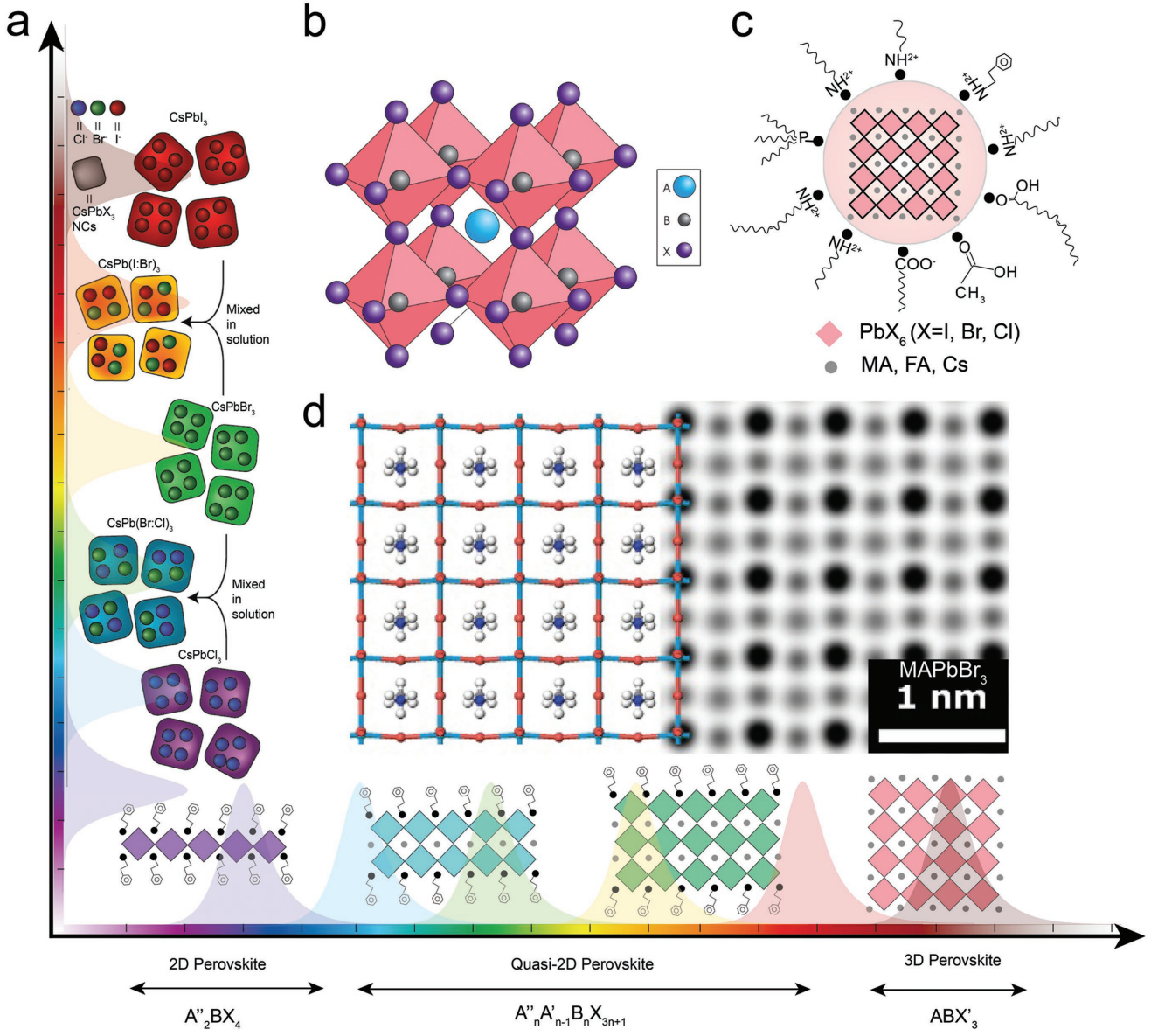


**Figure 1.** Controlling perovskite structure for band and exciton engineering. a) Schematic representation of bandgap-tunable perovskites by halide exchange and dimensionality engineering. Reproduced with permission.[42] Copyright 2015, American Chemical Society. b) Crystal structure of 3D $ABX_3$ perovskite. Reproduced with permission.[9] Copyright 2014, Nature Publishing Group. c) Ligand engineering of perovskite nanocrystals. d) High-resolution transmission electron microscopy image of $MAPbBr_3$ perovskites. c,d) Reproduced with permission.[21] Copyright 2018, AAAS.

demonstrated with the characteristic Burstein–Moss band filling model.[62]

Nevertheless, the existence of excitons has also been detected, including the presence of a large polarization-dependent exciton optical Stark effect.[63] Spectrally resolved transient absorption microscopy revealed the presence of small pockets (≈100 nm length scale) of exciton-dominated areas within an individual grain. In addition, the excitonic character can be increased with larger excitation densities[55] or by changing the structure of the perovskite. For instance, bromine-based 3D perovskites exhibit much higher exciton binding energies (67–150 meV),[64] resulting in higher excitonic character.[65] Similar effects can be observed with low-dimensional perovskites. An iodine-based 2D perovskite has shown an approximate exciton binding energy of ≈320 meV,[32] with quasi-2D perovskites bridging the values between 2D and 3D.[66,67]

After the initial excitation, the ground and excited states exist in a superposition over a given dephasing time. For 3D $CH_3NH_3PbI_3$, the dephasing time was found to be 220 fs, over 3× longer than in GaAs.[68] The dephasing time was found to be independent of the number of carriers, indicating that carrier–carrier scattering is negligible in the measured range. For quasi-2D iodine-based perovskites, many-body scattering was instead found to dominate, and the dephasing time was observed to decrease with decreasing confinement.[69]

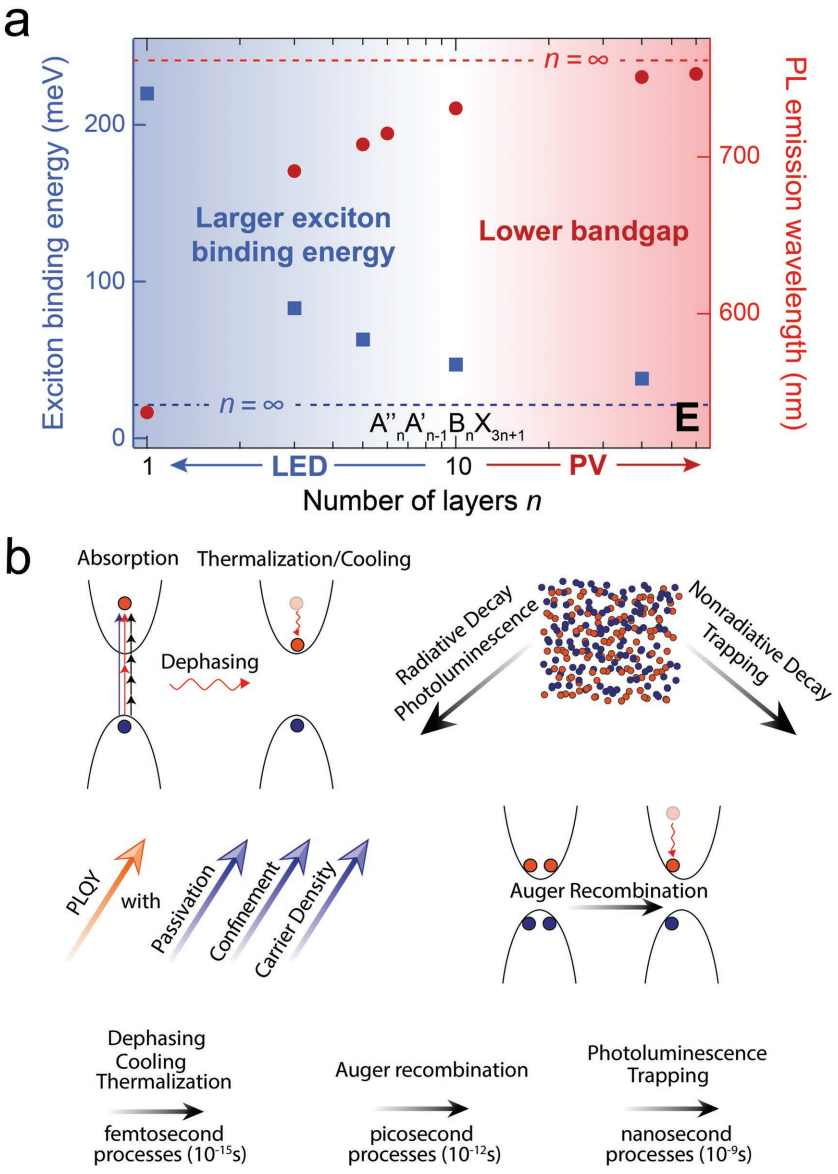


**Figure 2.** Photophysics in perovskites. a) Exciton binding energy and PL emission wavelength both decrease as a function of number of layers. b) Photophysical processes that occur after excitation of light. Auger recombination and other nonradiative rates can compete with photoluminescence.

After dephasing, the resulting excited state population then thermalizes (i.e., exchanges energy between charge carriers) and undergoes carrier cooling (Figure 2). In $CH_3NH_3PbI_3$, thermalization was found to occur mainly through carrier–carrier scattering, with thermalization times from under 10 to 85 fs.[70] Carrier cooling then proceeds at timescales over 100 fs.[71,72] At high photoexcitation densities, this can be dramatically increased by the phonon bottleneck effect,[72–74] where a cooling lifetime of ≈300 ps was reported in the case of $FAPbI_3$.[73] A separate 45 ps decay process was observed for $CH_3NH_3PbI_{3-x}Cl_x$, for excitations with energy larger than 2.38 eV;[75] this was attributed to an organic-to-inorganic sublattice thermalization process.

With the completion of ultrafast processes, competition begins between radiative decay (i.e., photoluminescence) and nonradiative decay. In perovskites, the nonradiative pathway is ascribed to charge trapping.[12] While trapping severely limits the PLQY of 3D perovskites at low fluences, radiative recombination dominates at high fluences (due to a large number of carriers), resulting in PLQYs near unity.[76] This improvement was extended to LEDs; however, due to a lack of charge confinement, the EQEs still remained modest.[11] Charge confinement was then introduced in $CH_3NH_2PbBr_3$ by reducing the grain size, which increased the radiative rate, and an EQE of 8.5% was achieved in the visible region.[77]

To achieve high PLQYs at low excitation density, investigation began into 2D perovskites, which have stable excitons at room temperature. Unfortunately, while the PLQY at low temperatures was near 100%, only low PLQY was reached at room temperature.[78] This was tentatively ascribed to thermal quenching of excitons.[18] Additionally, traps were shown to become more significant as the perovskite dimensionality was decreased from 3D to 2D.[79] Nevertheless, mixed-phase quasi-2D perovskites were shown to exhibit high PLQYs and EQEs for both near-IR[16,66] and visible[16,80] emission. The improved emission was caused by an energy funnel, where the charges were localized in the lowest-energy phases, allowing radiative recombination to outcompete trapping.[66] For perovskite nanocrystals, surface traps can also hamper PLQY, and passivating halide-ion pair ligands has been shown to improve performance.[81]

At high pump fluences, radiative decay must also compete with Auger recombination. Here, the additional energy is lost quickly due to thermal cooling, and the number of excitons diminishes, lowering the PLQY. Auger recombination increases with the exciton binding energy (i.e., confinement); for this reason, the rate of Auger recombination increases from 3D to 2D[82] and from iodine-based to bromine-based perovskites.[83] Likewise, as confinement is increased, the biexciton absorption redshifts to a greater extent in both single[84] and mixed domains.[69]

In this high fluence regime, Auger recombination competes with both spontaneous and stimulated emission. Lasing is perovskites was first observed in a 2D material, although only at temperatures below 40 K.[85] Room-temperature lasing was first observed in 3D $CH_3NH_3PbI_{3-x}Cl_x$ perovskite with a threshold of 0.2 µJ per pulse when a 400 ps pump was employed.[86] Continuous-wave lasing in $CH_3NH_3PbI_3$ was recently reported at 100 K, a temperature at which the orthorhombic phase is present.[87] Above 160 K, the tetragonal phase exists, and the limit to lasing duration has been attributed to a photoinduced structural change that reduces gain on a timescale of less than a microsecond.

**Table 1.** Photophysical study of perovskites.

| Material | Dimensionality | Photophysical insight | Ref. |
|---|---|---|---|
| $CH_3NH_3PbI_{3-x}Cl_x$ | 3D | High-energy phonon modes temporarily increase the rate of PL until organic-to-inorganic sublattice thermalization occurs | [149] |
| $CH_3NH_3PbI_3$ | 3D | Ultrafast carrier thermalization (8–85 fs) leads to fast dephasing of excited states | [70] |
| $(CH_3(CH_2)_3NH_3)_2(CH_3NH_3)_{x-1}Pb_xI_{3x+1}$ | Quasi-2D | Mixed phases align in the order of *n* perpendicular to the substrate | [150] |
| $CH_3NH_3PbI_3$ | 3D | Geminate recombination dominates at high fluences and early times while nongeminate recombination dominates at low excitation fluences and at late times | [59] |
| $CsPbX_3$[X = Cl, Br, I] | 3D | Biexcitonic redshift of ≈30 nm. Bandedges are twofold degenerated | [60] |
| $(C_{10}H_7CH_2NH_3)(CH_5N_2)PbI_4$ | Quasi-2D | Mixed phase induced higher exciton recombination decay rate and efficiency than bimolecular recombination in 3D perovskites | [67] |
| $CH_3NH_3PbBr_xI_{3-x}$ | 3D | Excitonic relation and quantum-beating signal with dephasing time of ≈40 fs | [45] |
| $CH_3NH_3PbI_3$ | 3D | Bandedge recombination is second order. Burstein–Moss band filling occurs | [62] |
| $(C_6H_5C_2H_4NH_3)_2(CH_3NH_3)_{x-1}Pb_xI_{3x+1}$ | Quasi-2D | Mixed phase quasi-2D perovskites induce funneling to lowest-bandgap emitter, increasing radiative recombination and PLQY | [66] |
| $CH_3NH_3PbI_{3-x}Cl_x$ | 3D | Charge-trapping pathways limit PLQY at low fluence. Efficiency approaches 100% at high fluences due to trap filling | [76] |
| $CH_3NH_3PbX_3$[X = Br, I] | 3D | Bimolecular recombination and Auger recombination are greater in Br-based perovskites than in I-based perovskites, due to larger exciton binding energies | [83] |
| $CH_3NH_3PbX$[X = $I_{3-x}Cl_x$, $Br_3$) | 3D | Higher PLQY at high excitation densities correlate with increased quantum efficiencies of LEDs at high current densities. First example of 3D perovskite LED operating at RT | [11] |
| $CH_3NH_3PbBr_3$ | 3D | Reducing the grain size increases the photoluminescence lifetime and PLQY due to spatial confinement of the injected charges | [77] |
| $CH_3NH_3Pb_3$ | 3D | Optical properties are better described with the free-carrier model than the exciton model | [61] |
| $CH_3NH_3PbI_3$, $(C_4H_9NH_3I)_2(CH_3NH_3I)_{x-1}(PbI_2)_x$ | 3D, quasi-2D, 2D | Excitonic traps are more enhanced as dimensionality is changed from 3D to 2D | [79] |
| $(RNH_3)_2(CH_3NH_3)_{x-1}A_xX_{3x+1}$ | 3D, quasi-2D, 2D | Lower-dimensional perovskites exhibit structural relaxation, PL shift, and higher PLQY than bulk | [78] |
| $C_6H_5C_2H_4NH_3)_2PbI_4$ | 2D | EL efficiency drops with increasing temperature, presumably due to thermal quenching | [98] |
| $(C_6H_{13}NH_3)_2PbI_4$ | 2D | First example of lasing in perovskites | [85] |
| $CH_3NH_3PbI_{3-x}Cl_x$ | 3D | Photoexcitation results in ≈1 ps free charge carrier formation and bimolecular recombination on times scales of 10–100 ns. First example of lasing in trihalide perovskite | [86] |
| $CH_3NH_3PbI$ | 3D | Perovskite matrix can transfer energy to embedded PbS quantum dots, due to epitaxial growth | [105] |
| $CsPbX_3$[X = Br, Cl] | 0D | Passivating QDs with halide and mixed halide ion pairs increases PLQY and EQE | [81] |
| $CsPbBr_xI_{3-x}$ | 0D | Compared to CdSe of similar volume, perovskite QDs have an ≈1 order of magnitude faster Auger lifetime but ≈3 times higher biexciton binding energy | [46] |

Indeed, the current record for pure photonic lasing in perovskites above this threshold is ≈100 ns at 200 K.[88] Similarly, for polariton lasing, continuous-wave operation is limited to low temperatures,[89] while room temperature lasing has so far been pulsed.[90]

## 4. Strategies Toward Improved Perovskite Light Emission

### 4.1. Composition and Grain Engineering

Improve perovskite composition has led to impressive strides in efficiency and stability in photovoltaics. Compositional engineering strategies can analogously be used to increase perovskite PL efficiencies, such as to control grain size and reduce surface trap density (**Table 2**).[91,92]

In late 2014, Friend and co-workers reported perovskite LEDs with halide mixed $CH_3NH_3PbI_{3-x}Cl_x$ that overcame the low exciton binding energy of 3D perovskites, and fabricated ultrathin and uniform films using the halide mixed strategy for green and red emission.[11] The resulting LEDs exhibited a 0.76% EQE and a 13.2 W $sr^{-1}$ $m^{-2}$ radiance at 773 nm near-infrared wavelength. Lee and co-workers engineered the methylammonium bromide (MABr) molar proportion in $MAPbBr_3$ green-emitting perovskite films, which prevented the formation of metallic lead (Pb) atoms that

**Table 2.** Photoluminesence quantum yield (PLQY) of perovskite films.

| Emitting materials | Dimensionality | PL wavelength [nm] | PLQY [%] | Excitation power [mW cm$^{-2}$] | Ref. |
|---|---|---|---|---|---|
| $MAPbBr_3$ | 3D | 540 | 36 | 30 | [77] |
| $MAPbI_{3-x}Cl_x$ | 3D | 754 | 26 | 33.3 | [11] |
| $MAPbBr_3$ | 3D | 524 | 7 | 33.3 | [11] |
| $CsPbBr_3$–poly(ethylene oxide) (PEO) | 3D | 521 | 60 | – | [146] |
| $(BAI)_{0.4}MAPbI_3$ | Quasi-2D | 730 | 6.6 | 4 | [16] |
| $(BABr)_{0.4}MAPbBr_3$ | Quasi-2D | 515 | 40.1 | 4 | [16] |
| $(FPMAI)_{0.2}$ $MAPbI_3$ | Quasi-2D | 749 | 4.4 | 2 | [147] |
| $(PEABr)_{0.2}$ $MAPbBr_3$ | Quasi-2D | 515 | 10.9 | 2 | [147] |
| $NMA_2FAPb_2I_6Br$ | Quasi-2D | 765 | 67 | 0.3 | [119] |
| $NMA_2FAPb_2Br_7$ | Quasi-2D | 518 | 20 | 0.3 | [119] |
| $(PEA)_2MA_2Pb_3I_{10}$ | Quasi-2D | 680 | 10.6 | 6 | [66] |
| $(PEA)_2PbBr_4$ | 2D | 407 | 27 | – | [148] |

caused strong exciton quenching.[77] $MAPbBr_3$ nanograins (≈100 nm) were formed by a nanocrystal pinning process with [2,2′,2″-(1,3,5-benzinetriyl)-tris(1-phenyl-1-*H*-benzimidazole)] (TPBi) additives and concomitant reduction of exciton diffusion length to 67 nm. Trap-assisted recombination—mostly occurring at grain boundaries—and radiative recombination inside the grains were found to dependent greatly on grain size. Small grain–sized $MAPbBr_3$ showed a PLQY of 36% compared to 3% for standard $MAPbBr_3$. This approach led to the highest EQE of 8.5% and 10 000 cd m$^{-2}$ luminance. A similar approach was used with stoichiometry-controlled $CsPbBr_3$ perovskite from the same group, with a device showing a maximum EQE of 1.37% with a luminance of 13 752 cd m$^{-2}$.[93]

Park and co-workers further explored this effect and reported a method to achieve highly luminescent $MAPbBr_3$ films based on nonstoichiometric adduct and solvent-vacuum drying processes.[94] This work presented the device performance of 8.2% EQE and 6950 cd m$^{-2}$ luminance. Zhang et al. reported Cs/MA mixed system for perovskite LEDs, and both film uniformity and PLQYs were enhanced due to the better control of crystallization kinetics of the $CsPbBr_3$ film by introducing MA cation. The device with $Cs_{0.87}MA_{0.13}PbBr_3$ perovskite exhibited 10% of EQE and 91 000 cd m$^{-2}$ of luminance.[95]

Rand and co-workers reported new methods to reduce the perovskite grains down to tens of nanometer sizes by introducing long bulky ligands in 3D perovskites to control their crystallization kinetics.[16] They incorporated butylammonium halide ligand as a surfactant that dramatically constrained the growth rate of the perovskites phase. The maximum PLQY from iodide perovskite ($\lambda$ = 750 nm) was 6.6% and bromide perovskite ($\lambda$ = 516 nm) was 40%. The highest EQEs reached 10.4% for 20:100 (butylammonium iodide to $MAPbI_3$) and 9.3% for 20:100 (butylammonium bromide to $MAPbBr_3$) LEDs.

Cation mixture (i.e., $CA^+$, $MA^+$, and $FA^+$) strategies have also been successfully employed to shift the emission wavelength from green to blue; this contrasts with halide mixture approaches that resulted in phase segregation and compromised stability.[96] The mixed-composition system is in line with other reports that used triplet-cation halide mixed $Cs_{10}(MA_{0.17}FA_{0.83})_{(100-x)}Pb(Br_xI_{1-x})_3$ perovskite and exhibited high-quality perovskite films and high device performances.[97]

### 4.2. Structural Engineering and Energy Manipulation

A chief challenge in the realization of efficient perovskite light emission has been the rather low efficient radiative recombination—a direct consequence of the low exciton binding energy and large charge mobility in conventional 3D perovskites. The spatial co-localization of electrons and holes in layered 2D perovskites, as well as the higher exciton binding energy, would, in principle, suggest the need for ultrathin films and/or confined grains. However, early reports in the 1990s observed electroluminescence from 2D perovskite films only at a relatively high fields (10 kV cm$^{-1}$) along the wells only below 200 K.[18,98] This is due to the larger scattering rate due to phonons at higher temperature which suppress the acceleration of electrons and/or holes. Their luminescence has failed to compete successfully with nonradiative processes.

Recently, researchers investigated a platform of mixed-organic, dimensionally tuned quasi-2D perovskite $PEA_2(MA)_{n-1}Pb_nI_{3n+1}$ (phenylethylammonium, PEA; $CH_3NH_3$, MA, methylammonium) thin films that continuously bridge the gap between 2D and 3D materials (**Figure 3**).[66] The dimensionality of this material was tuned by varying the ratio of methylammonium iodide (MAI) to PEAI. Members of the quasi-2D family combine the superior stability of 2D perovskites with optoelectronic parameters, such as long-range photocarrier diffusion, characteristic of 3D perovskites. This led to the realization of optoelectronic devices with improved stability.

The average number of layers $\langle n \rangle$ in quasi-2D perovskites, which make up the energy funneled structure, can be used as a means to enhance the PLQY. Specifically, a perovskite mixed material comprising a series of differently quantum-size-tuned grains funnels photoexcitations to the lowest-bandgap light emitter in the mixture.

LEDs built using quasi-2D perovskite as the active layer exhibited an EQE of 8.8% and a radiance of 80 W sr$^{-1}$ m$^{-2}$ at the near-infrared wavelengths (Figure 3c,d). The high performance was attributed to an inhomogeneous energy landscape that favored funneling of energy into domains with lower bandgap (Figure 3a).

A quantitative model of this phenomenon, together with a design strategy to unlock further advances in performance, was developed using $PEA_2(MA)_{n-1}Pb_nBr_{3n+1}$ perovskites as a model system.[80] When energy funnels from high bandgap domains into a small subpopulation of lower bandgap domains, radiative recombination outcompetes nonradiative recombination. By designing the energy landscape in quasi-2D

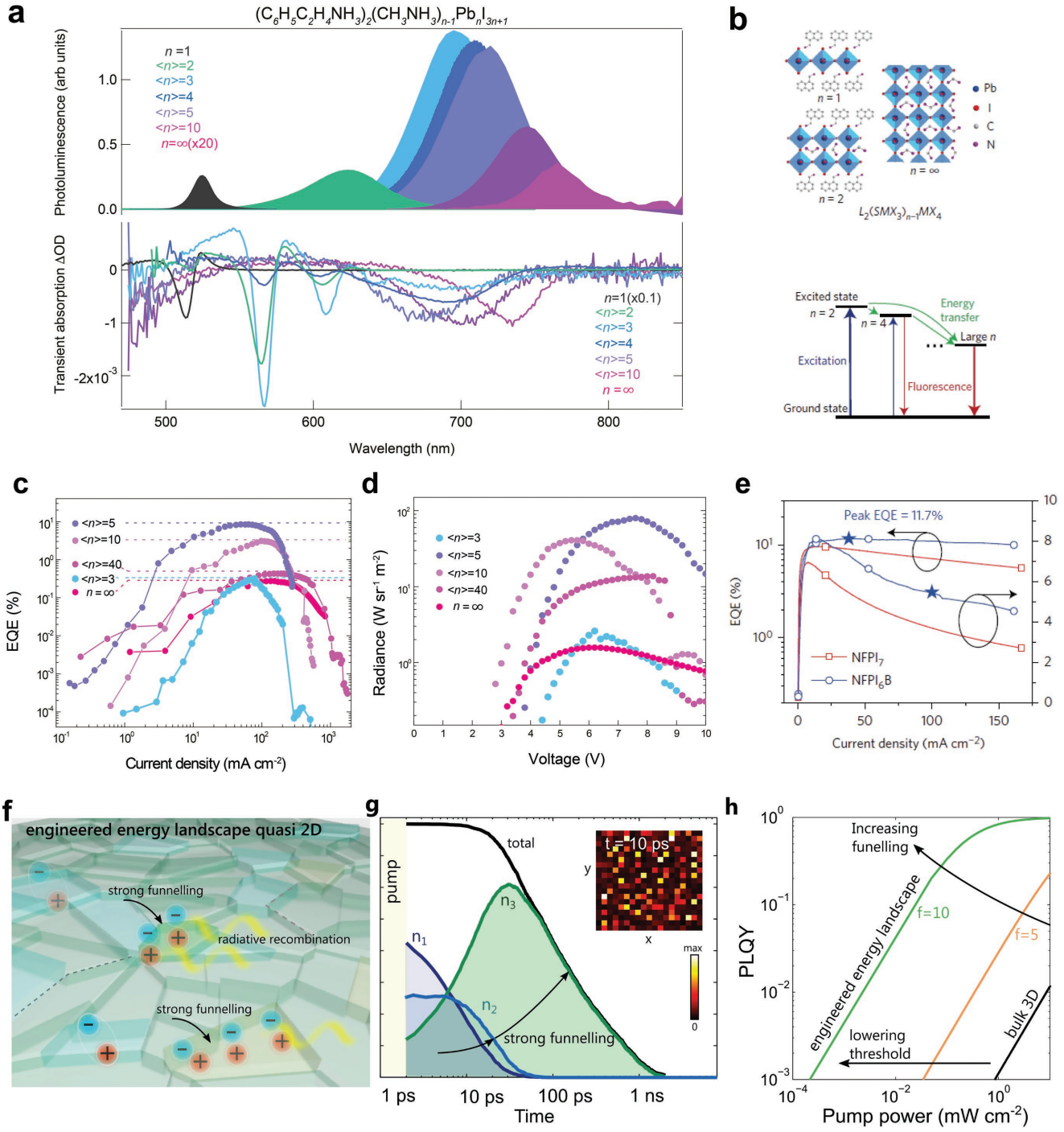


**Figure 3.** Energy landscape engineering in reduced-dimensional perovskites. a) Photoluminescence and transient absorption spectra for low-dimensional perovskites of $PEA_2(MA)_{n-1}Pb_nI_{3n+1}$. b) Energy transfer mechanisms in low-dimensional perovskites. c–e) Perovskite LED performances with low-dimensional perovskites. a,c,d) Reproduced with permission.[66] Copyright 2016, Nature Publishing Group. b,e) Reproduced with permission.[119] Copyright 2016, Nature Publishing Group. f–h) Strategy for engineering the grade of energy funnel in low-dimensional perovskites. f–h) Reproduced with permission.[80] Copyright 2016, American Chemical Society.

perovskites, researchers created green-emitting perovskite LEDs with 7.3% EQE and 8400 cd $m^{-2}$ luminance. Tisdale and co-workers reported that the addition of excess ligand could be used to achieve bluer emission.[99] By tuning the thickness of the layers, they built LEDs with blue emission utilizing the lead bromide system and orange emission utilizing the lead iodide system.

The wide tunability of the optical properties of multilayered perovskites entails the opportunity to implement transparent light-emitting displays by virtue of engineering the energy

funnel through wide bandgap domains into a small population of donor emitting domains.[100]

### 4.3. Composite Perovskite Systems

Another strategy to improve light emission is to separate the photo/electrical excitation and emission mechanisms, in such a way that two otherwise-entangled processes can be optimized independently. One may incorporate light emitters into a host matrix that supports charge/energy transport into embedded emitters (**Figure 4**a). This requires that two key requirements be met simultaneously: 1) homogeneous incorporation of emitters into the matrix without aggregation, and 2) preservation of the emitters' PLQY in the final configuration, i.e., the emitters must retain good passivation. This strategy, previously employed in other material systems such as quantum dot/organic semiconductor mixtures, has thus far been limited by the unstructured and defect-rich interface between these materials.

To manage the film uniformity and smoothness, several groups have explored the introduction of polymer additives in the perovskite film. Luminescent $MAPbBr_3$ nanocrystals embedded in a pinhole-free matrix of dielectric polymer (polyimide)[101] have been investigated by Li et al., and $CsPbBr_3$ perovskite mixed with poly(ethylene oxide)[102] has shown enhanced brightness (53 525 cd $m^{-2}$) and device performances (4.26% of EQE). Other polymers (i.e., poly(9-vinylcarbazole)[103] and poly(ethylene glycol))[104] have been mixed with perovskite in films.

A solution-processed semiconducting composite consisting of quantum dots, epitaxially embedded in metal halide perovskites, has been recently reported that meets these requirements.[105] To realize this material, researchers first exchanged the ligands of the quantum dots to be passivated instead with perovskite precursors, and then transferred the dots into a polar solvent such as dimethylformamide (DMF). The remaining perovskite precursors were then added to the solution at the desired ratio and stoichiometry. The perovskite phase then crystallized from the colloidal quantum dot (CQD) surface when processed using conventional perovskite formation techniques.[106] At the correct stoichiometry conditions, quantum dots became epitaxially incorporated into the perovskite matrix. This resulted in a PLQY similar to that of as-synthesized, oleic acid–capped CQDs, a signature of excellent passivation not previously obtained within a semiconducting CQD film.

Using this platform, Gong et al. engineered the compositional distribution of the mixed halide perovskite matrix and achieved a record electroluminescence power conversion efficiency (Figure 4b).[107,108] This represented a twofold improvement over previously reported CQD near-infrared LEDs. In this work, precise control over the CQD/perovskite interface was key to improving passivation and epitaxy. Yang et al. further explored this material and, by including alkylammonium/alkylamine substitution in the CQD surface during exchange, incorporated CQDs within a 2D perovskite matrix.[109] This single-step method resulted in more uniform, ≈40 nm thickness, films and a tenfold reduction in material usage compared to standard quantum-dot-in-perovskites.

Such a strategy can be applied to incorporate perovskite NC emitters into another crystalline transport phase (Figure 4c). Quan et al. embedded $CsPbBr_3$ quantum dots into a robust and air-stable rhombic prism hexabromide $Cs_4PbBr_6$ microcrystal phase.[110] Using modeling, they explored the importance of lattice matching between the NCs and the matrix, and achieved in this way improved passivation that ultimately led to a PLQY of 90% at 520 nm.

## 5. Perovskite LED Challenges

### 5.1. Effect of MHPs' Film Morphology

The film formation method, as well as the quality of the resulting MHPs, is a critical determinant of the electro-optical properties of MHPs. Uniform, smooth perovskite films are a requisite for high performance. Key factors include the choice of precursors, solvents, annealing conditions, and drying conditions as well as of deposition method.[111] Perovskite film-to-film repeatability is a key factor for reproducible LED fabrication (**Figure 5**, **Table 3**). The antisolvent dripping methods developed by Seok and co-workers have been widely used not only for solar cells but also in LED fabrication.[6] This method represented a significant improvement toward repeatable formation of high-quality films and devices compared to prior processes based on two-step spin-coating. However, the antisolvent method is sensitive to the speed, volume, and time of solvent dripping, as well as to deposition environment. Further advances in increasing film-to-film repeatability are therefore of interest. One recent advance included the incorporation of submicrometer crystalline perovskite seeds that, in a lead halide layer, improve the crystallization of the resulting perovskite once alkylammonium halides are added.[112]

Interfacial engineering approaches can promote the growth of a high-quality perovskite layers. Pinhole-free, high-uniformity (<5 nm surface roughness) perovskite crystals are a prerequisite for good device performance. A widely used strategy to improve the quality of the MHPs in LEDs is to incorporate a multifunctional polyethyleneimine (PEI) interlayer between the perovskite and oxide ETL.[113] Another is to blend the MHP film with a dielectric polyimide precursor (PIP) matrix. Each method helps to improve the morphology of the perovskite film, reduce nonradiative current losses, and increase EQE.[101]

### 5.2. Efficient Electrical Excitation

The low exciton binding energy within 3D MHPs is a factor that curtails the achievement of highly efficient LEDs.[57,114] The perovskite layer, when designed to be thin, will instead desirably spatially confine electrons and holes for efficient recombination. The confinement of injected charges within such a thin well structure could also enhance the electron–hole capture and improve radiative recombination.[11] The balanced energy levels of electron and hole injection layers will be crucial to efficient charge injection. Several strategies have been used to engineer the interfaces between the perovskite and electron–hole transport layers to improve the electrical excitation in perovskite devices.[113,115–118]

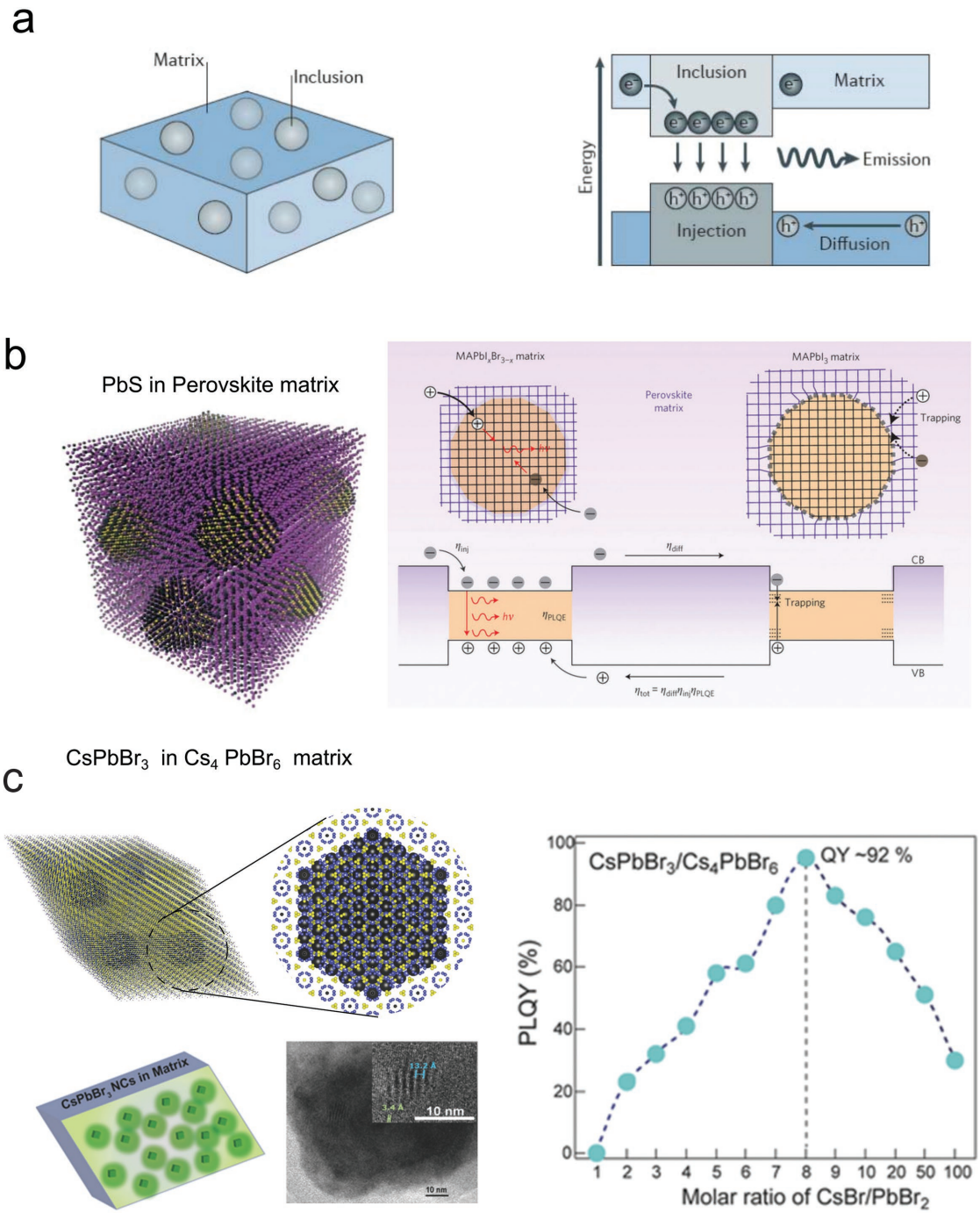


**Figure 4.** Hybrid perovskites for light emission. a) The inclusion of light-emitting materials within a host matrix that provides for charge/energy transport allows decoupling material photo/electrical excitation and radiative recombination. Reproduced with permission.[108] Copyright 2017, Nature Publishing Group. b) This leads to the parallel optimization of both properties, breaking the high-PLQY/transport compromise. Reproduced with permission.[105] Copyright 2015, Nature Publishing Group. c) Quantum-dot-in-perovskite solids are a new class of material consisting of quantum dots evenly embedded into a metal halide perovskite in an epitaxial fashion. This material combines the excellent transport properties of perovskites with quantum tunable light emission. Reproduced with permission.[110] Copyright 2017, Wiley-VCH.

Nonideal surface passivation and poor film formation have resulted in lower efficiencies than for bulk MHPs at forming LEDs. Tuning the dimensionality of perovskites has been used to improve the radiative recombination and transport in the perovskite layers. Quasi-2D perovskites have shown promising transport property and PL efficiency. The perovskite LEDs based on the quasi-2D perovskites boosted EQEs over 10%.[119]

All-inorganic $CsPbX_3$ perovskite NCs possess larger exciton binding energies than their bulk counterparts.[120] The best perovskite NC LEDs based on the $CsPbBr_3$ exhibited an emission

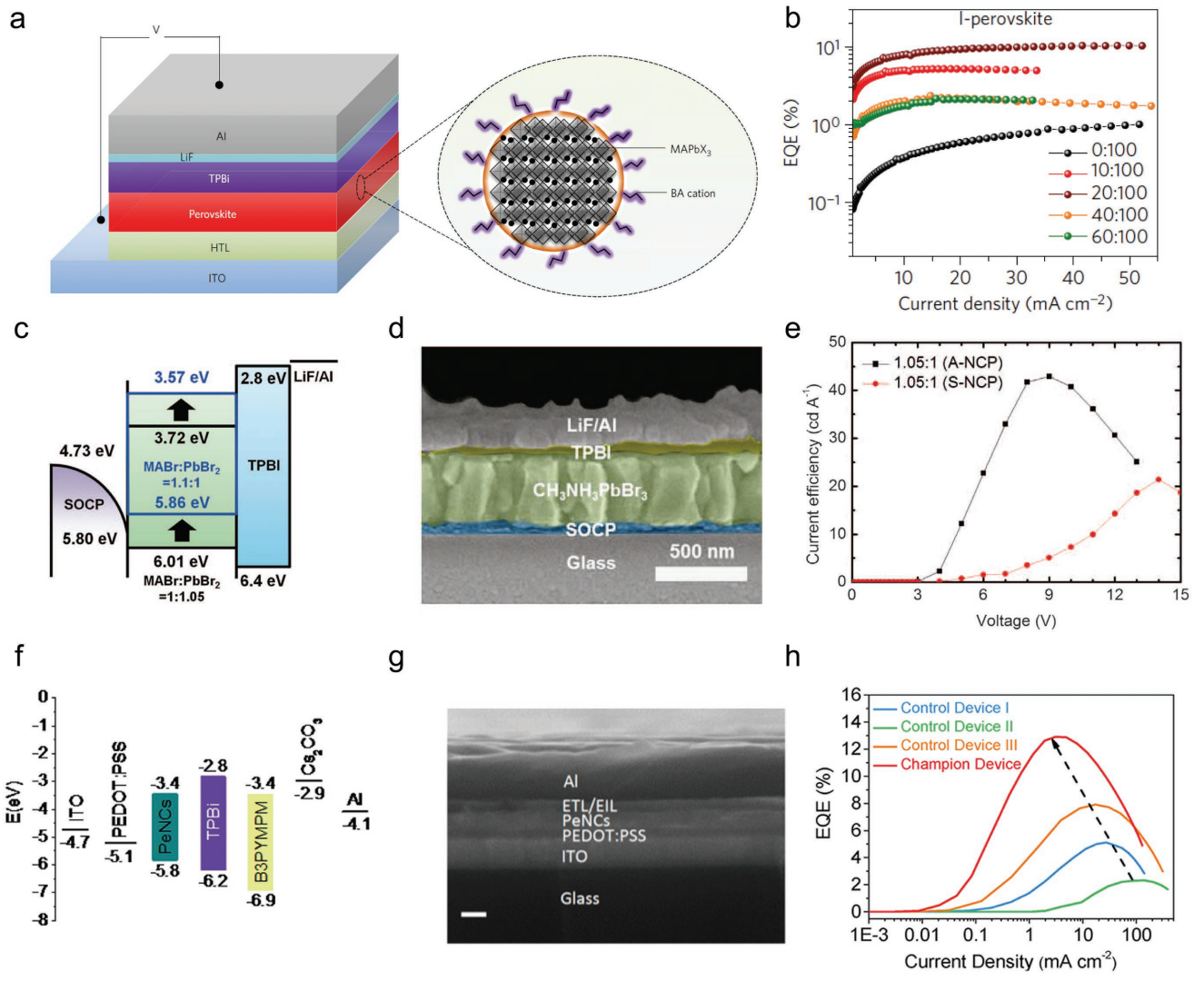


**Figure 5.** Perovskite LED structures and performance. a,c,f) Schematic representation of grain size engineered perovskite LEDs structure. d,g) For the device cross-sectional SEM image[77,117] and b,e,h) the device performance.[16,77,117] a,b) Reproduced with permission.[16] Copyright 2017, Nature Publishing Group; c–e) Reproduced with permission.[77] Copyright 2015, AAAS; f–h) Reproduced with permission.[117] Copyright 2018, American Chemical Society.

linewidth of 20 nm and near 15 000 cd $m^{-2}$ brightness and >6% EQE.[121]

MHPs show reduced Auger losses that distinguish them from other solution-processed materials, otherwise dominated by this deleterious recombination mechanism at high carrier densities. Nevertheless, perovskite LEDs still require high charge densities for efficient radiative recombination to occur due to the competing nonradiative trapping pathways. The removal or filling of these trap states by optimizing film formation and morphology would lead to enhanced device emission and quantum efficiency.

### 5.3. Toward Blue LEDs

Efficient blue light emission using metal halide perovskites remains as the major challenge in the field both from a material and a device perspective. The larger bandgap could, in principle, be achieved via Br–Cl halide mixtures; however, this is known to produce phase segregation, redshifting and broadening the emission wavelength, and leading to deteriorated optoelectronic properties.[96] On the other hand, 2D perovskite blue emitters can achieve the PLQY up to 79% and a linewidth of 20 nm; this high-brightness perovskites could move toward the potential application in blue light sources.[122] Blue emitters based on low-dimensional perovskites (0D and 2D) typically incorporate a large amount of organic ligands, deteriorating the electrical injection and transport within the active material.[99]

From a device perspective, selecting the optimum HTL and ETL for blue active material is another stringent requirement. The wide bandgap of the perovskite emitter limits the materials available to serve as HTL and ETL, especially since these must possess an appropriate mobility, valence band, and conduction band to implement balanced current injection (**Figure 6**d).

**Table 3.** Performance of perovskite LEDs (from red to blue).

| Year | Emitting materials | Device architecture[a)] | EL [nm] RGB | Peak EQE [%] | $L_{max}$ [cd m$^{-2}$]/$R_{max}$[b)] [W sr$^{-1}$ m$^{-2}$] | $T_{50}$ stability | Ref. |
|---|---|---|---|---|---|---|---|
| Red-near IR | | | | | | | |
| 2017 | $(BAI)_{0.2}MAPbI_3$ | ITO/polyTPD/perov/TPBi/LiF/Al[a)] | 748 | 10.4 | 30 | 90 s @5 V | [16] |
| 2017 | $(FPMAI)_{0.2}$ $MAPbI_3$ | ITO/polyTPD/perov/TPBi/LiF/Al | 749 | 7.9 | 72$^R$ | 10 h @3 mA cm$^{-2}$ | [147] |
| 2017 | $Cs_{10}MA_{0.17}FA_{0.83}Pb(Br_{1-x}I_x)_3$ | ITO/ZnO/perov/NPD/$MoO_3$/Al | 750 | 9.23 | 93.34$^R$ | – | [91] |
| 2017 | $MAPbI_{1.05}Br_{1.95}$ | ITO/PEDOT:PSS/peorv/Ca:ZnO/Ca/Al | 635 | 5.8 | 1000 | – | [116] |
| 2016 | $NMA_2FAPb_2I_6Br$ | ITO/ZnO/PEIE/perov/TFB/$MoO_x$/Au | 786 | 11.7 | 82$^R$ | 25 min@10 mA cm$^{-2}$ | [119] |
| 2016 | $PEA_2MA_4Pb_5I_{16}$ | ITO/$TiO_2$/perov/F8/$MoO_x$/Au | 750 | 8.8 | 80 | – | [66] |
| 2015 | $MAPbI_{3-x}Cl_x$ | ITO/ZnO/PEIE/perov/TFB/$MoO_x$/Au | 768 | 3.5 | 28$^R$ | – | [113] |
| 2014 | $MAPbI_{3-x}Cl_x$ | ITO/$TiO_2$/perov/F8/$MoO_x$/Au | 773 | 0.76 | 13.2$^R$ | – | [11] |
| Green | | | | | | | |
| 2017 | $Cs_{0.87}MA_{0.13}PbBr_3$ | ITO/ZnO/PVP/perov/CBP/$MoO_3$/Al | 520 | 10.43 | 91 000 | 40 s @3.7 V | [95] |
| 2017 | $MAPbBr_3$ | ITO/PEDOT:PSS/peorv/TPBi/LiF/Al | 530 | 8.2 | 6950 | 100 s@6.5 V | [94] |
| 2017 | $(BABr)_{0.2}MAPbBr_3$ | ITO/PVK/perov/TPBi/LiF/Al | 513 | 9.3 | 2900 | 90 s @5 V | [16] |
| 2017 | $(PEABr)_{0.2}$ $MAPbBr_3$ | ITO/PVK/perov/TPBi/LiF/Al | 515 | 7.0 | 11 400 | 5 min@3 mA cm$^{-2}$ | [147] |
| 2017 | $Cs_{10}MA_{0.17}FA_{0.83}Pb(Br_{1-x}I_x)_3$ | ITO/ZnO/perov/NPD/$MoO_3$/Al | 569 | 7.3 | 19 420 | 135 min@3 mA cm$^{-2}$ | [91] |
| 2017 | $MAPbBr_3$ | ITO/PEDOT:PSS/peorv/Ca:ZnO/Ca/Al | 540 | 6.2 | 300 | – | [116] |
| 2017 | $MAPbBr_3$ | Graphene/PEDOT:PSS:PFI/perv/TPBi/LiF/Al | 542 | 3.8 | 13 000 | – | [115] |
| 2016 | $NMA_2FAPb_2Br_7$ | ITO/ZnO/PEIE/perov/TFB/$MoO_x$/Au | 518 | 0.1 | – | – | [119] |
| 2016 | $FAPbBr_3$ | ITO/ZnO/perov/poly-TPD/$MoO_3$/Al | 540 | 1.16 | 13 062 | – | [114] |
| 2016 | $MAPbBr_3$ | ITO/PEDOT:PSS/peorv/SPW-111/LiF/Ag | 540 | 5.1 | 7850 | – | [135] |
| 2016 | $CsPbBr_3$–PEO | ITO/PEDOT:PSS/peorv/TPBi/LiF/Al | 521 | 4.26 | 53 525 | – | [102] |
| 2016 | $MAPbBr_3$ | Glass/PEDOT:PSS:PFI/peorv/TPBi/LiF/Al | 542 | 8.53 | 10 000 | – | [77] |
| 2015 | $MAPbBr_3$:PIP | ITO/PEDOT:PSS/peorv/F8/Ca/Ag | 534 | 1.2 | 200 | – | [101] |
| 2015 | $MAPbBr_3$ | ITO/PEDOT:PSS:PFI/peorv/TPBi/LiF/Al | 540 | 0.125 | 417 | – | [15] |
| Blue | | | | | | | |
| 2017 | $Cs_{10}MA_{0.17}FA_{0.83}Pb(Cl_{1-x}Br_x)_3$ | ITO/ZnO/perov/NPD/$MoO_3$/Al | 475 | 1.7 | 3567 | 25 min@3 mA cm$^{-2}$ | [97] |
| 2016 | $(PEA)_2PbBr_4$ | ITO/PEDOT:PSS/perov/TPBi/Ca/Al | 410 | 0.04 | – | – | [148] |
| 2014 | $MAPbI_{3-x}Cl_x$ | ITO/PEDOT:PSS/peorv/F8/Ca/Ag | 532 | 0.1 | 364 | | [11] |
| Perovskite nanocrystals | | | | | | | |
| Red | | | | | | | |
| 2017 | $FAPbI_3$ nanocrystal | ITO/PEDOT:PSS/peorv/TPBi/LiF/Al | 692 | 2.3 | 1.54 | – | [92] |
| 2016 | $CsPbI_3$ nanocrystal | ITO/ZnO/perov/TFB/$MoO_3$/Ag | 698 | 5.7 | 206 | – | [111] |
| 2016 | $CsPbI_{2.25}Br_{0.75}$ nanocrystal | ITO/ZnO/perov/TFB/$MoO_3$/Ag | 619 | 1.4 | 1559 | – | [111] |
| Green | | | | | | | |
| 2018 | $MAPbBr_3$ nanocrystal | ITO/PEDOT:PSS/peorv/TPBi/B3PYMPM/$Cs_2CO_3$/Al | 524 | 12.9 | 22 830 | – | [117] |
| 2018 | $(OA)_2(FA)_{n-1}Pb_nBr_{3n+1}$ | ITO/PEDOT:PSS/peorv/TPBi/PO-T2T/Ca/Al | 530 | 13.4 | 34 480 | 400 s@105 cd m$^{-2}$ | [100] |
| 2017 | $CsPbBr_3$ nanocrystal | ITO/PEDOT:PSS/poly-TPD/peorv/TPBi/LiF/Al | 515 | 6.27 | 15 000 | – | [121] |
| 2017 | $MAPbBr_3$ nanocrystal | ITO/PEDOT:PSS:PFI/peorv/TPBi/LiF/Al | 520 | 6.27 | 1000 | – | [39] |
| 2017 | $FA_{0.8}Cs_{0.2}PbBr_3$ nanocrystal | ITO/PEDOT:PSS/peorv/TPBi/LiF/Al | 525 | 2.8 | 55 005 | – | [40] |
| 2016 | $CsPbX_3$ nanocrystal | ITO/PEDOT:PSS/PVK/peorv/TPBi/LiF/Al | 515 | 3.0 | 330 | – | [81] |
| 2016 | $MAPbBr_3$ nanocrystal | ITO/PEDOT:PSS/Poly-TPD/peorv/B3PYMPM/$Cs_2CO_3$/Al | 512 | 3.8 | 3515 | 30 s @100 cd m$^{-2}$ | [118] |
| 2016 | $CsPbBr_3$ nanocrystal | ITO/ZnO/perov/TFB/$MoO_3$/Ag | 523 | 0.19 | 2335 | – | [111] |

**Table 3.** Continued.

| Year | Emitting materials | Device architecture[a)] | EL [nm] RGB | Peak EQE [%] | $L_{max}$ [cd m$^{-2}$]/$R_{max}$[b)] [W sr$^{-1}$ m$^{-2}$] | $T_{50}$ stability | Ref. |
|---|---|---|---|---|---|---|---|
| 2015 | $CsPbX_3$ nanocrystal | ITO/PEDOT:PSS/PVK/peorv/TPBi/LiF/Al | 516 | 0.12 | 946 | – | [120] |
| Blue | | | | | | | |
| 2016 | $CsPbX_3$ nanocrystal | ITO/PEDOT:PSS/PVK/peorv/TPBi/LiF/Al | 490 | 1.9 | 35 | – | [81] |
| 2016 | $CsPbBr_{1.5}Cl_{1.5}$ nanocrystal | ITO/ZnO/perov/TFB/$MoO_3$/Ag | 480 | 0.0074 | 8.7 | – | [111] |
| 2015 | $CsPbX_3$ nanocrystal | ITO/PEDOT:PSS/PVK/peorv/TPBi/LiF/Al | 455 | 0.07 | 742 | – | [120] |

[a)]ITO = indium tin oxide; PEDOT:PSS = poly(3,4-ethylenedioxythiophene:polystyrene sulfonate); NPD = *N*,*N*′-bis(naphthalen-1-yl)-*N*,*N*′-bis(phenyl)benzidine; PEIE = polyethylenimine ethoxylated; CBP = 4,4-*N*,*N*′-dicarbazole-1,1′-biphenyl; TPD = *N*,*N*′-bis(3-methylphenyl)-*N*,*N*′-diphenylbenzidine; PVK = poly(9-vinylcarbazole); [b)]*R* = radiance.

Inefficient electron/hole blocking could also lead to high current leakage and diminished EQE. Blue perovskite LEDs made with $Cs_xMA_{0.17}FA_{0.83}Pb(Br_{3-x}Cl_x)_3$ perovskites exhibit 475 nm emission wavelength, and the device shows 1.7% of EQE and 3567 cd m$^{-2}$ in luminance.[97] However, phase segregation of Br and Cl mixed perovskite under high-voltage stress deteriorates the device performance and the stability. Jin and co-workers used pure phase 2D perovskite $(PEA)_2PbBr_4$ for violet perovskite LEDs and reported a 0.038% EQE. The low conductivity of 2D perovskites arising due to organic barriers resulted in low brightness and high current density in the device. Lower-dimensional blue-emitting perovskite NCs have been implemented in LEDs showing a higher EQE 1.9% but accompanied by a low luminance around 35 cd m$^{-2}$.[81] More recently, Congreve and co-workers have used $CsPbBr_xCl_{3-x}$ perovskite for blue LEDs, and demonstrated that emission efficiency and lifetime are significantly decreased when $NiO_x$ was used as HTL.[123] Combination of bilayered poly[(9,9-dioctylfluorenyl-2,7-diyl)-*co*-(4,4′-(*N*-(4-*sec*-butylphenyl) diphenylamine)] (TFB) and Nafion perfluorinated ionomer (PFI), which does not affect the photoluminescence of nanocrystals and overall boosts efficiency, enabled performance of 0.5% EQE for 469 nm emitting devices.

Remaining material challenges in blue perovskite LED include the need to address halide induced phase separation under the operating stress; the requirement to improve

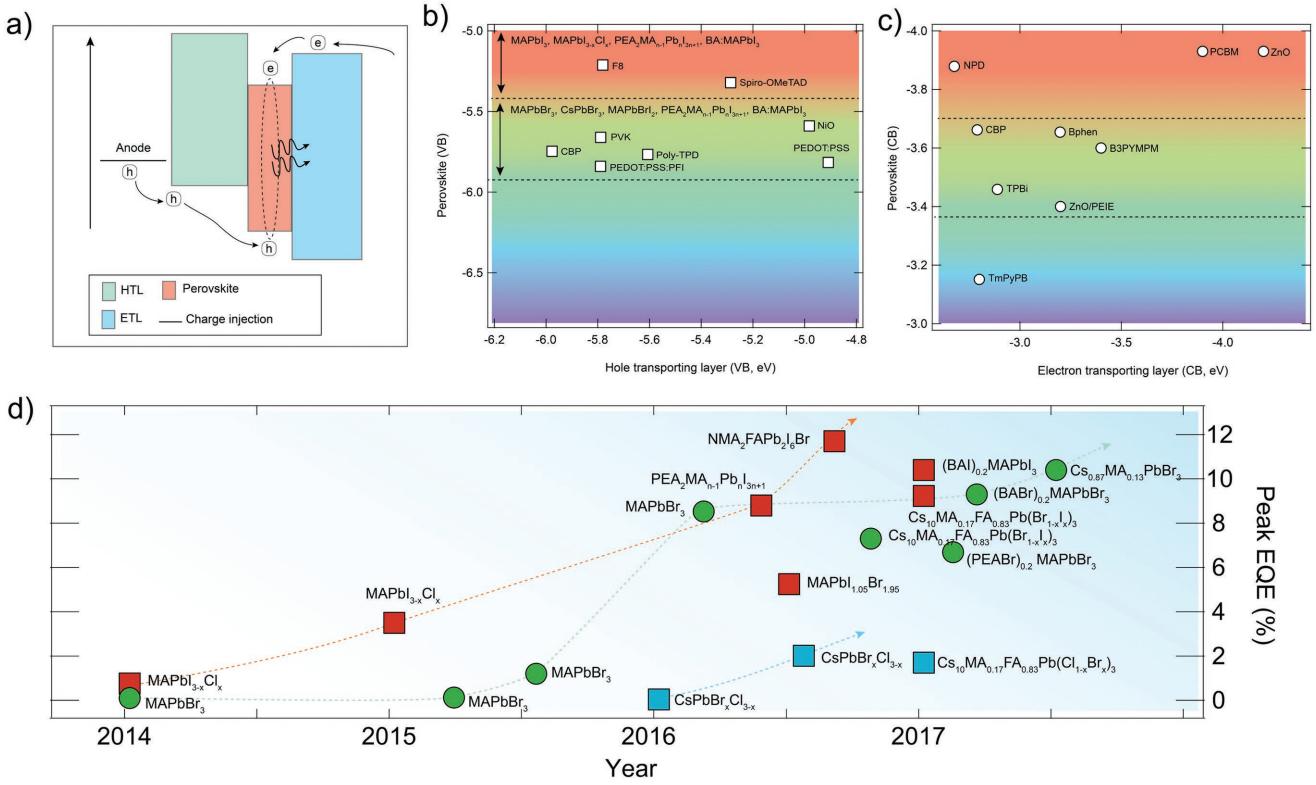


**Figure 6.** Electron- and hole-injecting layers and the resultant performance of red, green, blue (RGB) perovskite LEDs. a) Schematic representation of perovskite LEDs' working principle, b) selected hole-transporting layers, and c) electron-transporting layers in perovskite LEDs for bandgap-tunable materials, and d) the state-of-the-art device external quantum efficiency chart for perovskite LEDs.

conductivity in layered perovskite material systems; and the need to improve charge injection balance in perovskite NC devices to maximize LED luminance.

### 5.4. White Light Emission in Perovskites

2D perovskites have also shown promise for white light emission.[124,125] White light–emitting 2D perovskites are attracting increasing interest for solid-state light emission applications. Broad white light emission originates from trapped exciton recombination rather than from band-edge free exciton emission.[125]

Early reports of white light–emitting perovskites from Karunadasa and co-workers relied on the use of (N-MEDA)$PbBr_4$ and (EDBE)$PbX_4$ (N-MEDA: N1-methylethane-1,2-diammonium; EDBE: 2,2′-(ethylenedioxy)bis(ethylammonium) with a 2D-layered crystal structure.[126] These crystals, which possess a wide bandgap, emit photons with energies across the visible spectrum. As exciton self-trapping is the primary source of the broad Stokes-shifted PL in 2D perovskites, researchers have tried to improve understanding of these photophysical mechanisms. For example, the broad emission of (EDBE)$PbBr_4$ becomes much narrower with decreasing temperature, as the vibrational coupling contributes significantly to the emission linewidth. Remarkably, the PLQY of (EDBE)$PbBr_4$ perovskites increases from 9% at 300 K to 85% at 105 K. Yuan et al. reported white light emission from a $C_4N_2H_{14}PbBr_4$ perovskite, which has 1D structure.[127] This led to strong quantum confinement with an increased formation of self-trapped excited states that gave rise to more efficient and bluer white light emission. The PLQY for bulk single crystals was ≈20%, whereas microscale crystals exhibited a PLQY of 12%.

Further advances in the field of white light emission are to be expected by deepening understanding of the self-trapping mechanisms and opening thereby strategies to enhance the absolute PLQY at room temperature.

### 5.5. The Stability Challenge

While the efficiency of perovskite LEDs has swiftly risen to more than 10%, the operating lifetimes are far below those of inorganic quantum dot LEDs (QD LEDs) and organic LEDs (OLEDs). In contrast with perovskite solar cells, whose device lifetimes now exceed 1000 h under continuous operation,[128] reported operational lifetimes of perovskite LEDs remain yet impractical, reaching at most the minutes range under continuous electrical stress. In contrast, QD LEDs exhibit lifetimes on the order of 100–1000 h when operated at mild brightness (1000 cd $m^{-2}$).[17] This is still below the stringent requirements of commercial displays over >10 000 h at a higher brightness of 3000 cd $m^{-2}$.

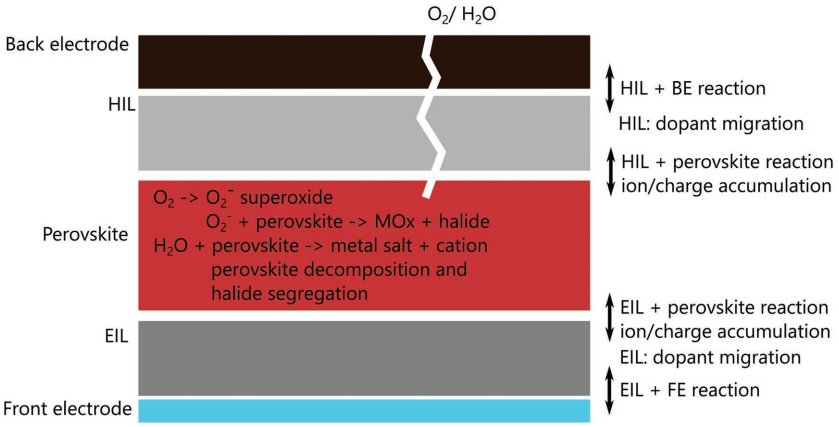


**Figure 7.** Degradation pathways within perovskite LEDs. Degradation of metal halide perovskite LEDs can proceed through different pathways. Direct degradation of the active layer takes place via superoxide generation leading to perovskite decomposition; moisture-induced decomposition, and phase segregation and spontaneous decomposition. Degradation from the device level occurs through EIL/HIL degradation induced by electrochemical reactions with mobile ions. Dopant migration as well as oxygen and moisture penetration into the perovskite active material represents a limiting operational factor for long-term stability, highlighting the importance of a chemically robust inert encapsulation.

In contrast, the lifetime of state-of-the-art OLEDs is in the range of 10 000–100 000 h. For early generations of OLEDs, the instability was triggered by dark-spot effects, but soon device encapsulation and manufacturing optimization overcame the stability issues.[129]

In this section, we discuss the origin of device instability in perovskite LEDs, and the connection between fundamental aspects such as the strong ionic character of perovskites, their low formation energy, and the electrochemistry occurring at the interfaces with considerations at the device level (**Figure 7**).

#### *5.5.1. Materials' Moisture–Thermal–Photo Stability*

One of the major factors curtailing the stability of metal halide perovskites is their low formation energy. Metal halide perovskite thin films lack chemical and structural stability, and thus are prone to undergo rapid degradation in the presence of moisture or heat. The strong ionic character of MHPs causes mixed halide perovskites to phase segregate when exposed to light, favoring oxygen-catalyzed photochemical reactions.[130]

*Moisture*: In 2014, researchers turned their attention to stabilizing the perovskite against moisture and sought to exploit the hydrophobic nature of bulky organic ligands. Based on this approach, Smith et al. reported a layered hybrid perovskite solar cell with enhanced moisture stability.[35] They used a perovskite composition of $(PEA)_2(MA)_2[Pb_3I_{10}]$. Due to the hydrophobic nature of the PEA layers, this material was far more resistant to moisture compared to its 3D analog. Using a computational approach, Quan et al. proposed that the intercalation of PEA between perovskite layers would introduce quantitatively appreciable van der Waals interactions. These would drive an increased formation energy that could potentially lead to improved materials stability.[37] Based on these findings, the authors demonstrated experimentally the dependence of

moisture-induced degradation on perovskite composition and dimensionality. The introduction of additives such as butylammonium halides,[131] butylphosphonic acid ammonium additives,[132] poly(dimethylsiloxane)–urea copolymers,[133] and thiourea[134,137] has also been reported to improve device performance and to slow the degradation of 3D perovskites.

*Temperature*: The intrinsic and extrinsic effects of temperature are crucial in accelerating perovskite degradation. At the high current densities relevant to LED operation (≈100 mA $cm^{-2}$), the temperature in the recombination zone can rise up at least 60 °C. From a device perspective, this limits the maximum external and internal efficiencies attainable in devices when Joule heating is at play. The development of perovskite materials that exhibit exceptional thermal stability is of paramount importance for highly efficient, bright LEDs.[135] One, particularly, interesting class of metal halide perovskites consists of $CsPbX_3$. Schaller and co-workers reported that the resilience of perovskite PL at temperatures below 450 K depends strongly on halide composition.[136] Chloride-containing perovskite nanocrystals show consistently greater susceptibility to thermal quenching than pure bromide, iodide, or iodide–bromide-mixed halides. Pure $CsPbBr_3$ nanocrystals show the greatest thermal stability among the samples investigated, with bromide–iodide and pure iodide compounds substantially more stable than chloride-containing nanocrystals. PL loss in $CsPbBr_3$ nanocrystals indicated a mixture of reversible (to 450 K) and irreversible (>450 K) loss pathways. Yuan et al. reported $CsPbBr_3$ nanocrystals annealed in vacuum at various temperatures, finding that the nanocrystals exhibited significant thermal degradation of PL when annealed above 320 K.[137]

*Photodegradation*: The photoinstability of perovskites is yet to be understood and resolved. There are several degradation pathways of perovskite under illumination at various environmental conditions. Super-resolution luminescence microspectroscopy under intense light excitation has been used to study photoinduced degradation of $MAPbI_3$ perovskite crystals.[138] It has been observed that the degradation starts locally and then spreads over the whole crystal. The structural collapse is primarily due to migration of methylammonium ions ($MA^+$), which distorts the lattice structure and causes alterations to the Pb—I—Pb bond angle and in turn changes the bandgap. Yuan et al. observed that, at low excitation power densities, two-state blinking was found on individual perovskite nanorods with dimensions of several hundred nanometers.[138] Furthermore, a strong environmental dependence of nanorod PL blinking was revealed by comparing measurements made in vacuum, nitrogen, and air, and a finding also suggestive that traps locate close to crystal surfaces. The authors reasoned that surface charge traps are likely related to under-coordinated lead ions and methylammonium vacancies to result in the PL blinking.

The stability of $CH_3NH_3PbI_3$ perovskite films was also investigated by using visible and ultraviolet light in oxygen atmosphere and in vacuum. Light illumination on perovskite film in oxygen atmosphere results in an accelerated degradation. Oxygen molecules solely act as catalysts for the degradation mechanism by promoting the deprotonation process of methylammonium ions.[130]

Illumination of $CH_3NH_3PbI_3$ in vacuum was found to decrease amine concentration in the lattice. Recently, Aristidou et al. reported that fast oxygen diffusion into perovskite is accompanied by photoinduced formation of highly reactive superoxide species.[139] It is observed that oxygen diffusion into the perovskite films is remarkably fast for 500 nm thick perovskite film, reaching complete oxygen saturation within 10 min. This is especially true in perovskite films composed of small grains, which show higher yields of superoxide and thus lower stability. This is important information since small grains are preferred in perovskite LEDs. Photoinduced segregation in mixed halide lead perovskites is important to achieving stable LED performance.

The shift in the absorption and the rate of formation of iodide- and bromide-rich regions, following visible excitation of mixed halide lead perovskites, is found to depend strongly on halide ion concentration.[140] The halide ions can move within the perovskites, and this can destabilize mixed halide perovskites under long-term illumination.

Photogenerated polarons were found recently to localize in iodide-rich regions of $MAPb(I_{1-x}Br_x)_3$ film, leading to increased local lattice strain.[140] This results in the promotion of iodide migration and growth of iodide-rich domains. However, it was found that at excess halide concentration, segregation effects become less prominent, as evidenced by faster recovery kinetics. These results suggest that light-induced compositional segregation can be minimized in mixed halide perovskite films by using excess halide ions. Br—I mixed perovskites nevertheless retain considerable halide segregation.

#### 5.5.2. Device Operational Stability

Device operating stability remains approximately in the minutes range; orders of magnitude shorter than the best QLEDs and OLEDs.[16] The degradation process in perovskite LEDs that are under electrical stress requires investigation and resolution. Perovskite LEDs utilize a glass/ITO/PEDOT:PSS/perovskite/TPBi/LiF/Al architecture in light of the well-matched band alignment with the ETL and the HTL. However, the acidic nature of PEDOT:PSS and electrochemically reactive LiF and Al exacerbate device instability.[141]

Recently, device degradation was explained as an electrochemical reaction at the device interfacs (Figure 7). Zhao et al. reported degradation and decomposition of devices investigated using in situ scanning electron microscopy (SEM) and X-ray diffraction (XRD) measurements.[142] The redox reaction occurs spontaneously when Al is in direct contact with $MAPbI_3$, even in the absence of external factors such as light, moisture, or oxygen.

For perovskite LEDs at ≈90% relative humidity (RH), complete degradation is observed within 2 min, whereas no apparent degradation is observed in 2 h in dry air. The *J–V* curve at 27% RH shows that the leakage current is increased by 5 orders of magnitude within 6 min, indicating a dramatic degradation of the diode related to the degradation of the active layers and/or their interfaces. If a device is exposed to high humidity for 3–4 h, well beyond the point of performance degradation, the entire device stack, including the Al electrode,

becomes transparent. However, the interlayer such as TPBi or LiF serves only to separate physically the Al and perovskite. Devices showed similar degradation and were rendered transparent. The hydrophobicity of the interlayer may also influence the device degradation rate. Moreover, Guerrero et al. reported that under dry ambient conditions, devices degraded dramatically following illumination of 1 sun for 4 h.[143] $I^-$ from perovskite layer contributes to the corrosion of the Ag metal contacts.[144]

Domanski et al. found that exposing perovskite devices to a temperature of 70 °C is sufficient to induce gold metal electrode migration through the HTL, 2,2′,7,7′-tetrakis[*N*,*N*-di(4-methoxyphenyl)amino]-9,9′-spirobifluorene (spiro-MeOTAD), and into the perovskite material, which in turn severely affects device performance metrics under working conditions.[145] However, with the introduction of a Cr metal interlayer between the HTL and gold electrode, high temperature–induced irreversible long-term losses are avoided. The problem of metal-induced degradation is not resolved completely by sealing the devices; metal diffusion must be stopped, presumably via the use of an alternative HTL or an interfacial layer that prevents this phenomenon. Back et al. reported a similar approach to prevent degradation of perovskite devices that was seen even under inert conditions; they used a chemical inhibition layer of amine-mediated titanium suboxide on perovskites.[141] The metal electrodes were successfully protected, and the ionic defects stabilized within the perovskite layer.

Hysteresis in perovskite solar cells is well known under continuous operation and is ascribed to halide ion migration and associated traps. Cho et al. have studied the origins of hysteresis in perovskite LEDs due to $Br^-$ ion migration.[93] Using temperature-dependent EL investigations, they concluded that the origins of decreased spectral area, spectral blueshift, and linewidth broadening are related to $Br^-$ anion migration, thermal dissociation of excitons, thermal expansion, and electron–phonon interaction. Xiao et Al. performed scan rate–dependent *J*–*V*–*L* measurement on perovskite LEDs with and without bulky-organic ligand–capped perovskites.[16] The organic chains of butylammonium cations that self-assemble at the crystallite surface either impede ion motion or prevent ions from within crystallites from participating in ion migration processes, leading to increased device stability.

## 6. Conclusion and Outlook

A wide structural diversity within the metal-halide perovskites makes them a compelling material platform well suited to applications as next-generation light emitters. Low-dimensional perovskites present additional benefits of excitonic behavior and high radiative recombination, and offer an avenue to increased stability. Reduced-dimensional perovskites offer a route to manipulate the quantum-well energy landscape, a feature that can be used to direct energy transfer into a small fraction of emitting domains, further strengthening radiative recombination and opening the door to transparent bright light–emitting displays. Rapid enhancements to perovskite LED efficiency have been achieved from perovskite compositional, surface, and structural engineering. Although high EQEs for red and green LEDs have already been reported consistently, efficient blue perovskite LEDs are still a challenge, with EQEs today limited to the approximately low percent regime. The operational stability of perovskite LEDs is very low today compared to that of technologies such as QLEDs and OLEDs. White light emission has also the potential to benefit from the use of low-dimensional perovskites. More efforts are still needed to increase the yet moderate quantum efficiency and to shed light on the photophysical mechanisms that lead to white light emission perovskites. Low-dimensional perovskites in particular offer a promising route to overcome these limitations by virtue of their superior stability and the high degree of tunability.

## Acknowledgements

This article is part of the *Advanced Materials* Hall of Fame article series, which recognizes the excellent contributions of leading researchers to the field of materials science.

## Conflict of Interest

The authors declare no conflict of interest.

## Keywords

halide perovskites, layered perovskites, light-emitting diodes, light-emitting materials, reduced dimensional perovskites, Ruddlesden–Popper perovskites

Received: March 28, 2018
Revised: May 26, 2018
Published online:

[1] H. S. Kim, C. R. Lee, J. H. Im, K. B. Lee, T. Moehl, A. Marchioro, S. J. Moon, R. Humphry-Baker, J. H. Yum, J. E. Moser, M. Gratzel, N. G. Park, *Sci. Rep.* **2012**, *2*, 591.
[2] D. Shi, V. Adinolfi, R. Comin, M. Yuan, E. Alarousu, A. Buin, Y. Chen, S. Hoogland, A. Rothenberger, K. Katsiev, *Science* **2015**, *347*, 519.
[3] W. Li, Z. Wang, F. Deschler, S. Gao, R. H. Friend, A. K. Cheetham, *Nat. Rev. Mater.* **2017**, *2*, 16099.
[4] A. Kojima, K. Teshima, Y. Shirai, T. Miyasaka, *J. Am. Chem. Soc.* **2009**, *131*, 6050.
[5] M. M. Lee, J. Teuscher, T. Miyasaka, T. N. Murakami, H. J. Snaith, *Science* **2012**, *338*, 643.
[6] N. J. Jeon, J. H. Noh, Y. C. Kim, W. S. Yang, S. Ryu, S. I. Seok, *Nat. Mater.* **2014**, *13*, 897.
[7] J. Burschka, N. Pellet, S. J. Moon, R. Humphry-Baker, P. Gao, M. K. Nazeeruddin, M. Gratzel, *Nature* **2013**, *499*, 316.
[8] N. J. Jeon, J. H. Noh, W. S. Yang, Y. C. Kim, S. Ryu, J. Seo, S. I. Seok, *Nature* **2015**, *517*, 476.
[9] M. A. Green, A. Ho-Baillie, H. J. Snaith, *Nat. Photonics* **2014**, *8*, 506.
[10] O. D. Miller, E. Yablonovitch, S. R. Kurtz, *IEEE J. Photovoltaics* **2012**, *2*, 303.
[11] Z. K. Tan, R. S. Moghaddam, M. L. Lai, P. Docampo, R. Higler, F. Deschler, M. Price, A. Sadhanala, L. M. Pazos, D. Credgington,

F. Hanusch, T. Bein, H. J. Snaith, R. H. Friend, *Nat. Nanotechnol.* **2014**, *9*, 687.
[12] G. Xing, N. Mathews, S. S. Lim, N. Yantara, X. Liu, D. Sabba, M. Grätzel, S. Mhaisalkar, T. C. Sum, *Nat. Mater.* **2014**, *13*, 476.
[13] H. Zhu, Y. Fu, F. Meng, X. Wu, Z. Gong, Q. Ding, M. V. Gustafsson, M. T. Trinh, S. Jin, X. Y. Zhu, *Nat. Mater.* **2015**, *14*, 636.
[14] F. Liu, Y. Zhang, C. Ding, S. Kobayashi, T. Izuishi, N. Nakazawa, T. Toyoda, T. Ohta, S. Hayase, T. Minemoto, K. Yoshino, S. Dai, Q. Shen, *ACS Nano* **2017**, *11*, 10373.
[15] Y. H. Kim, H. Cho, J. H. Heo, T. S. Kim, N. Myoung, C. L. Lee, S. H. Im, T. W. Lee, *Adv. Mater.* **2015**, *27*, 1248.
[16] Z. Xiao, R. A. Kerner, L. Zhao, N. L. Tran, K. M. Lee, T.-W. Koh, G. D. Scholes, B. P. Rand, *Nat. Photonics* **2017**, *11*, 108.
[17] X. Dai, Z. Zhang, Y. Jin, Y. Niu, H. Cao, X. Liang, L. Chen, J. Wang, X. Peng, *Nature* **2014**, *515*, 96.
[18] K. Chondroudis, D. B. Mitzi, *Chem. Mater.* **1999**, *11*, 3028.
[19] X. Yang, X. Zhang, J. Deng, Z. Chu, Q. Jiang, J. Meng, P. Wang, L. Zhang, Z. Yin, J. You, *Nat. Commun.* **2018**, *9*, 570.
[20] M. De Graef, M. E. McHenry, *Structure of Materials: an Introduction to Crystallography, Diffraction and Symmetry*, Cambridge University Press, Cambridge **2012**.
[21] D. Zhang, Y. Zhu, L. Liu, X. Ying, C.-E. Hsiung, R. Sougrat, K. Li, Y. Han, *Science* **2018**, *359*, 675.
[22] a) D. B. Mitzi, *J. Chem. Soc., Dalton Trans.* **2001**, 1; b) D. B. Mitzi, *Prog. Inorg. Chem.* **2007**, *48*, 1.
[23] L. Liang, L. Wencong, C. Nianyi, *J. Phys. Chem. Solids* **2004**, *65*, 855.
[24] a) J. H. Noh, S. H. Im, J. H. Heo, T. N. Mandal, S. I. Seok, *Nano Lett.* **2013**, *13*, 1764; b) C. C. Stoumpos, C. D. Malliakas, M. G. Kanatzidis, *Inorg. Chem.* **2013**, *52*, 9019.
[25] I. Borriello, G. Cantele, D. Ninno, *Phys. Rev. B* **2008**, *77*, 235214.
[26] M. R. Filip, G. E. Eperon, H. J. Snaith, F. Giustino, *Nat. Commun.* **2014**, *5*, 5757.
[27] E. Mosconi, A. Amat, M. K. Nazeeruddin, M. Grätzel, F. De Angelis, *J. Phys. Chem. C* **2013**, *117*, 13902.
[28] D. Mitzi, S. Wang, C. Feild, C. Chess, A. Guloy, *Science* **1995**, *267*, 1473.
[29] D. B. Mitzi, *Chem. Mater.* **1996**, *8*, 791.
[30] D. B. Mitzi, K. Chondroudis, C. R. Kagan, *IBM J. Res. Dev.* **2001**, *45*, 29.
[31] K. Tanaka, F. Sano, T. Takahashi, T. Kondo, R. Ito, K. Ema, *Solid State Commun.* **2002**, *122*, 249.
[32] X. Hong, T. Ishihara, A. Nurmikko, *Phys. Rev. B* **1992**, *45*, 6961.
[33] T. Fujita, Y. Sato, T. Kuitani, T. Ishihara, *Phys. Rev. B* **1998**, *57*, 12428.
[34] D. B. Mitzi, C. Feild, W. Harrison, A. Guloy, *Nature* **1994**, *369*, 467.
[35] I. C. Smith, E. T. Hoke, D. Solis-Ibarra, M. D. McGehee, H. I. Karunadasa, *Angew. Chem., Int. Ed.* **2014**, *126*, 11414.
[36] D. H. Cao, C. C. Stoumpos, O. K. Farha, J. T. Hupp, M. G. Kanatzidis, *J. Am. Chem. Soc.* **2015**, *137*, 7843.
[37] L. N. Quan, M. Yuan, R. Comin, O. Voznyy, E. M. Beauregard, S. Hoogland, A. Buin, A. R. Kirmani, K. Zhao, A. Amassian, *J. Am. Chem. Soc.* **2016**, *138*, 2649.
[38] L. Protesescu, S. Yakunin, M. I. Bodnarchuk, F. Krieg, R. Caputo, C. H. Hendon, R. X. Yang, A. Walsh, M. V. Kovalenko, *Nano Lett.* **2015**, *15*, 3692.
[39] M. Nirmal, L. Brus, *Acc. Chem. Res.* **1999**, *32*, 407.
[40] Y.-H. Kim, C. Wolf, Y.-T. Kim, H. Cho, W. Kwon, S. Do, A. Sadhanala, C. G. Park, S.-W. Rhee, S. H. Im, *ACS Nano* **2017**, *11*, 6586.
[41] X. Zhang, H. Liu, W. Wang, J. Zhang, B. Xu, K. L. Karen, Y. Zheng, S. Liu, S. Chen, K. Wang, *Adv. Mater.* **2017**, *29*, 1606405.
[42] Q. A. Akkerman, V. D'Innocenzo, S. Accornero, A. Scarpellini, A. Petrozza, M. Prato, L. Manna, *J. Am. Chem. Soc.* **2015**, *137*, 10276.
[43] a) F. Zhang, H. Zhong, C. Chen, X.-g. Wu, X. Hu, H. Huang, J. Han, B. Zou, Y. Dong, *ACS Nano* **2015**, *9*, 4533; b) H. C. Yoon, H. Kang, S. Lee, J. H. Oh, H. Yang, Y. R. Do, *ACS Appl. Mater. Interfaces* **2016**, *8*, 18189.
[44] Y. Kim, E. Yassitepe, O. Voznyy, R. Comin, G. Walters, X. Gong, P. Kanjanaboos, A. F. Nogueira, E. H. Sargent, *ACS Appl. Mater. Interfaces* **2015**, *7*, 25007.
[45] L. Wang, N. E. Williams, E. W. Malachosky, J. P. Otto, D. Hayes, R. E. Wood, P. Guyot-Sionnest, G. S. Engel, *ACS Nano* **2017**, *11*, 2689.
[46] J. A. Castañeda, G. Nagamine, E. Yassitepe, L. G. Bonato, O. Voznyy, S. Hoogland, A. F. Nogueira, E. H. Sargent, C. H. B. Cruz, L. A. Padilha, *ACS Nano* **2016**, *10*, 8603.
[47] N.-G. Park, *Mater. Today* **2015**, *18*, 65.
[48] W. S. Yang, B.-W. Park, E. H. Jung, N. J. Jeon, Y. C. Kim, D. U. Lee, S. S. Shin, J. Seo, E. K. Kim, J. H. Noh, S. I. Seok, *Science* **2017**, *356*, 1376.
[49] R. Zhang, J. Fan, X. Zhang, H. Yu, H. Zhang, Y. Mai, T. Xu, J. Wang, H. J. Snaith, *ACS Photonics* **2016**, *3*, 371.
[50] G. Walters, B. R. Sutherland, S. Hoogland, D. Shi, R. Comin, D. P. Sellan, O. M. Bakr, E. H. Sargent, *ACS Nano* **2015**, *9*, 9340.
[51] W. Liu, J. Xing, J. Zhao, X. Wen, K. Wang, P. Lu, Q. Xiong, *Adv. Opt. Mater.* **2017**, *5*, 1601045.
[52] W. Chen, S. Bhaumik, S. A. Veldhuis, G. Xing, Q. Xu, M. Grätzel, S. Mhaisalkar, N. Mathews, T. C. Sum, *Nat. Commun.* **2017**, *8*, 15198.
[53] W. G. Lu, C. Chen, D. Han, L. Yao, J. Han, H. Zhong, Y. Wang, *Adv. Opt. Mater.* **2016**, *4*, 1732.
[54] T. Hartmann, P. Reineker, V. Yudson, *Phys. Rev. B* **2011**, *84*, 245317.
[55] V. D'Innocenzo, G. Grancini, M. J. Alcocer, A. R. S. Kandada, S. D. Stranks, M. M. Lee, G. Lanzani, H. J. Snaith, A. Petrozza, *Nat. Commun.* **2014**, *5*, 3586.
[56] Q. Lin, A. Armin, R. C. R. Nagiri, P. L. Burn, P. Meredith, *Nat. Photonics* **2014**, *9*, 106.
[57] A. Miyata, A. Mitioglu, P. Plochocka, O. Portugall, J. T.-W. Wang, S. D. Stranks, H. J. Snaith, R. J. Nicholas, *Nat. Phys.* **2015**, *11*, 582.
[58] a) L. Q. Phuong, Y. Yamada, M. Nagai, N. Maruyama, A. Wakamiya, Y. Kanemitsu, *J. Phys. Chem. Lett.* **2016**, *7*, 2316; b) M. T. Trinh, X. Wu, D. Niesner, X. Y. Zhu, *J. Mater. Chem. A* **2015**, *3*, 9285.
[59] L. H. Manger, M. B. Rowley, Y. Fu, A. K. Foote, M. T. Rea, S. L. Wood, S. Jin, J. C. Wright, R. H. Goldsmith, *J. Phys. Chem. C* **2016**, *121*, 1062.
[60] J. Aneesh, A. Swarnkar, V. K. Ravi, R. Sharma, A. Nag, K. Adarsh, *J. Phys. Chem. C* **2017**, *121*, 4734.
[61] Y. Yamada, T. Nakamura, M. Endo, A. Wakamiya, Y. Kanemitsu, *J. Am. Chem. Soc.* **2014**, *136*, 11610.
[62] J. S. Manser, P. V. Kamat, *Nat. Photonics* **2014**, *8*, 737.
[63] Y. Yang, M. Yang, K. Zhu, J. C. Johnson, J. J. Berry, J. van de Lagemaat, M. C. Beard, *Nat. Commun.* **2016**, *7*, 12613.
[64] a) I. B. Koutselas, L. Ducasse, G. C. Papavassiliou, *J. Phys.: Condens. Matter* **1996**, *8*, 1217; b) K. Tanaka, T. Takahashi, T. Ban, T. Kondo, K. Uchida, N. Miura, *Solid State Commun.* **2003**, *127*, 619.
[65] C. Sheng, C. Zhang, Y. Zhai, K. Mielczarek, W. Wang, W. Ma, A. Zakhidov, Z. V. Vardeny, *Phys. Rev. Lett.* **2015**, *114*, 116601.
[66] M. Yuan, L. N. Quan, R. Comin, G. Walters, R. Sabatini, O. Voznyy, S. Hoogland, Y. Zhao, E. M. Beauregard, P. Kanjanaboos, *Nat. Nanotechnol.* **2016**, *11*, 872.
[67] G. Xing, B. Wu, X. Wu, M. Li, B. Du, Q. Wei, J. Guo, E. K. Yeow, T. C. Sum, W. Huang, *Nat. Commun.* **2017**, *8*, 14558.
[68] S. A. March, D. B. Riley, C. Clegg, D. Webber, X. Liu, M. Dobrowolska, J. K. Furdyna, I. G. Hill, K. C. Hall, *ACS Photonics* **2017**, *4*, 1515.
[69] M. H. Elkins, R. Pensack, A. H. Proppe, O. Voznyy, L. N. Quan, S. O. Kelley, E. H. Sargent, G. D. Scholes, *J. Phys. Chem. Lett.* **2017**, *8*, 3895.

[70] J. M. Richter, F. Branchi, F. Valduga de Almeida Camargo, B. Zhao, R. H. Friend, G. Cerullo, F. Deschler, *Nat. Commun.* **2017**, *8*, 376.
[71] P. Piatkowski, B. Cohen, F. Javier Ramos, M. Di Nunzio, M. K. Nazeeruddin, M. Gratzel, S. Ahmad, A. Douhal, *Phys. Chem. Chem. Phys.* **2015**, *17*, 14674.
[72] M. B. Price, J. Butkus, T. C. Jellicoe, A. Sadhanala, A. Briane, J. E. Halpert, K. Broch, J. M. Hodgkiss, R. H. Friend, F. Deschler, *Nat. Commun.* **2015**, *6*, 8420.
[73] J. Yang, X. Wen, H. Xia, R. Sheng, Q. Ma, J. Kim, P. Tapping, T. Harada, T. W. Kee, F. Huang, Y.-B. Cheng, M. Green, A. Ho-Baillie, S. Huang, S. Shrestha, R. Patterson, G. Conibeer, *Nat. Commun.* **2017**, *8*, 14120.
[74] Y. Yang, D. P. Ostrowski, R. M. France, K. Zhu, J. van de Lagemaat, J. M. Luther, M. C. Beard, *Nat. Photonics* **2015**, *10*, 53.
[75] A. Y. Chang, Y.-J. Cho, K.-C. Chen, C.-W. Chen, A. Kinaci, B. T. Diroll, M. J. Wagner, M. K. Y. Chan, H.-W. Lin, R. D. Schaller, *Adv. Energy Mater.* **2016**, *6*, 1600422.
[76] S. D. Stranks, V. M. Burlakov, T. Leijtens, J. M. Ball, A. Goriely, H. J. Snaith, *Phys. Rev. Appl.* **2014**, *2*, 034007.
[77] H. Cho, S.-H. Jeong, M.-H. Park, Y.-H. Kim, C. Wolf, C.-L. Lee, J. H. Heo, A. Sadhanala, N. Myoung, S. Yoo, S. H. Im, R. H. Friend, T.-W. Lee, *Science* **2015**, *350*, 1222.
[78] L. Dou, A. B. Wong, Y. Yu, M. Lai, N. Kornienko, S. W. Eaton, A. Fu, C. G. Bischak, J. Ma, T. Ding, N. S. Ginsberg, L.-W. Wang, A. P. Alivisatos, P. Yang, *Science* **2015**, *349*, 1518.
[79] X. Wu, M. T. Trinh, D. Niesner, H. Zhu, Z. Norman, J. S. Owen, O. Yaffe, B. J. Kudisch, X. Y. Zhu, *J. Am. Chem. Soc.* **2015**, *137*, 2089.
[80] L. N. Quan, Y. Zhao, F. P. Garcia de Arquer, R. Sabatini, G. Walters, O. Voznyy, R. Comin, Y. Li, J. Z. Fan, H. Tan, J. Pan, M. Yuan, O. M. Bakr, Z. Lu, D. H. Kim, E. H. Sargent, *Nano Lett.* **2017**, *17*, 3701.
[81] J. Pan, L. N. Quan, Y. Zhao, W. Peng, B. Murali, S. P. Sarmah, M. Yuan, L. Sinatra, N. M. Alyami, J. Liu, *Adv. Mater.* **2016**, *28*, 8718.
[82] R. L. Milot, R. J. Sutton, G. E. Eperon, A. A. Haghighirad, J. Martinez Hardigree, L. Miranda, H. J. Snaith, M. B. Johnston, L. M. Herz, *Nano Lett.* **2016**, *16*, 7001.
[83] Y. Yang, M. Yang, Z. Li, R. Crisp, K. Zhu, M. C. Beard, *J. Phys. Chem. Lett.* **2015**, *6*, 4688.
[84] T. Ishihara, X. Hong, J. Ding, A. V. Nurmikko, *Surf. Sci.* **1992**, *267*, 323.
[85] T. Kondo, T. Azuma, T. Yuasa, R. Ito, *Solid State Commun.* **1998**, *105*, 253.
[86] F. Deschler, M. Price, S. Pathak, L. E. Klintberg, D.-D. Jarausch, R. Higler, S. Hüttner, T. Leijtens, S. D. Stranks, H. J. Snaith, *J. Phys. Chem. Lett.* **2014**, *5*, 1421.
[87] Y. Jia, R. A. Kerner, A. J. Grede, B. P. Rand, N. C. Giebink, *Nat. Photonics* **2017**, *11*, 784.
[88] M. Cadelano, V. Sarritzu, N. Sestu, D. Marongiu, F. Chen, R. Piras, R. Corpino, C. M. Carbonaro, F. Quochi, M. Saba, A. Mura, G. Bongiovanni, *Adv. Opt. Mater.* **2015**, *3*, 1557.
[89] T. J. Evans, A. Schlaus, Y. Fu, X. Zhong, T. L. Atallah, M. S. Spencer, L. E. Brus, S. Jin, X. Y. Zhu, *Adv. Opt. Mater.* **2018**, *6*, 1700982.
[90] Y. Jia, R. A. Kerner, A. J. Grede, A. N. Brigeman, B. P. Rand, N. C. Giebink, *Nano Lett.* **2016**, *16*, 4624.
[91] M.-H. Park, S.-H. Jeong, H.-K. Seo, C. Wolf, Y.-H. Kim, H. Kim, J. Byun, J. S. Kim, H. Cho, T.-W. Lee, *Nano Energy* **2017**, *42*, 157.
[92] L. Protesescu, S. Yakunin, S. Kumar, J. Bar, F. Bertolotti, N. Masciocchi, A. Guagliardi, M. Grotevent, I. Shorubalko, M. I. Bodnarchuk, C. J. Shih, M. V. Kovalenko, *ACS Nano* **2017**, *11*, 3119.
[93] H. Cho, C. Wolf, J. S. Kim, H. J. Yun, J. S. Bae, H. Kim, J. M. Heo, S. Ahn, T. W. Lee, *Adv. Mater.* **2017**, *29*, 1700579.
[94] J. W. Lee, Y. J. Choi, J. M. Yang, S. Ham, S. K. Jeon, J. Y. Lee, Y. H. Song, E. K. Ji, D. H. Yoon, S. Seo, H. Shin, G. S. Han, H. S. Jung, D. Kim, N. G. Park, *ACS Nano* **2017**, *11*, 3311.
[95] L. Zhang, X. Yang, Q. Jiang, P. Wang, Z. Yin, X. Zhang, H. Tan, Y. M. Yang, M. Wei, B. R. Sutherland, E. H. Sargent, J. You, *Nat. Commun.* **2017**, *8*, 15640.
[96] A. Sadhanala, S. Ahmad, B. Zhao, N. Giesbrecht, P. M. Pearce, F. Deschler, R. L. Hoye, K. C. Godel, T. Bein, P. Docampo, S. E. Dutton, M. F. De Volder, R. H. Friend, *Nano Lett.* **2015**, *15*, 6095.
[97] H. P. Kim, J. Kim, B. S. Kim, H.-M. Kim, J. Kim, A. R. B. M. Yusoff, J. Jang, M. K. Nazeeruddin, *Adv. Opt. Mater.* **2017**, *5*, 1600920.
[98] M. Era, S. Morimoto, T. Tsutsui, S. Saito, *Appl. Phys. Lett.* **1994**, *65*, 676.
[99] D. N. Congreve, M. C. Weidman, M. Seitz, W. Paritmongkol, N. S. Dahod, W. A. Tisdale, *ACS Photonics* **2017**, *4*, 476.
[100] X. Y. Chin, A. Perumal, A. Bruno, N. Yantara, S. A. Veldhuis, L. Martínez-Sarti, B. Chandran, V. Chirvony, A. S.-Z. Lo, J. So, *Energy Environ. Sci.* **2018**, *11*, 1770.
[101] G. Li, Z. K. Tan, D. Di, M. L. Lai, L. Jiang, J. H. Lim, R. H. Friend, N. C. Greenham, *Nano Lett.* **2015**, *15*, 2640.
[102] J. Li, S. G. Bade, X. Shan, Z. Yu, *Adv. Mater.* **2015**, *27*, 5196.
[103] P. Chen, Z. Xiong, X. Wu, M. Shao, X. Ma, Z. H. Xiong, C. Gao, *J. Phys. Chem. Lett.* **2017**, *8*, 1810.
[104] L. Song, X. Guo, Y. Hu, Y. Lv, J. Lin, Z. Liu, Y. Fan, X. Liu, *J. Phys. Chem. Lett.* **2017**, *8*, 4148.
[105] Z. Ning, X. Gong, R. Comin, G. Walters, F. Fan, O. Voznyy, E. Yassitepe, A. Buin, S. Hoogland, E. H. Sargent, *Nature* **2015**, *523*, 324.
[106] F. P. G. de Arquer, X. Gong, R. P. Sabatini, M. Liu, G.-H. Kim, B. R. Sutherland, O. Voznyy, J. Xu, Y. Pang, S. Hoogland, *Nat. Commun.* **2017**, *8*, 14757.
[107] X. Gong, Z. Yang, G. Walters, R. Comin, Z. Ning, E. Beauregard, V. Adinolfi, O. Voznyy, E. H. Sargent, *Nat. Photonics* **2016**, *10*, 253.
[108] O. Voznyy, B. R. Sutherland, A. H. Ip, D. Zhitomirsky, E. H. Sargent, *Nat. Rev. Mater.* **2017**, *2*, 17026.
[109] Z. Yang, O. Voznyy, G. Walters, J. Z. Fan, M. Liu, S. Kinge, S. Hoogland, E. H. Sargent, *ACS Photonics* **2017**, *4*, 830.
[110] L. N. Quan, R. Quintero-Bermudez, O. Voznyy, G. Walters, A. Jain, J. Z. Fan, X. Zheng, Z. Yang, E. H. Sargent, *Adv. Mater.* **2017**, *29*, 1605945.
[111] G. Li, F. W. R. Rivarola, N. J. Davis, S. Bai, T. C. Jellicoe, F. de la Peña, S. Hou, C. Ducati, F. Gao, R. H. Friend, *Adv. Mater.* **2016**, *28*, 3528.
[112] Y. Zhao, H. Tan, H. Yuan, Z. Yang, J. Z. Fan, J. Kim, O. Voznyy, X. Gong, L. N. Quan, C. S. Tan, *Nat. Commun.* **2018**, *9*, 1607.
[113] J. Wang, N. Wang, Y. Jin, J. Si, Z. K. Tan, H. Du, L. Cheng, X. Dai, S. Bai, H. He, Z. Ye, M. L. Lai, R. H. Friend, W. Huang, *Adv. Mater.* **2015**, *27*, 2311.
[114] L. Meng, E. P. Yao, Z. Hong, H. Chen, P. Sun, Z. Yang, G. Li, Y. Yang, *Adv. Mater.* **2017**, *29*, 1603826.
[115] H. K. Seo, H. Kim, J. Lee, M. H. Park, S. H. Jeong, Y. H. Kim, S. J. Kwon, T. H. Han, S. Yoo, T. W. Lee, *Adv. Mater.* **2017**, *29*, 1605587.
[116] K. Qasim, B. Wang, Y. Zhang, P. Li, Y. Wang, S. Li, S. T. Lee, L. S. Liao, W. Lei, Q. Bao, *Adv. Funct. Mater.* **2017**, *27*, 1606874.
[117] F. Yan, J. Xing, G. Xing, L. N. Quan, S. T. Tan, J. Zhao, R. Su, L. Zhang, S. Chen, Y. Zhao, A. Huan, E. H. Sargent, Q. Xiong, H. V. Demir, *Nano Lett.* **2018**, *18*, 3157.
[118] J. Xing, F. Yan, Y. Zhao, S. Chen, H. Yu, Q. Zhang, R. Zeng, H. V. Demir, X. Sun, A. Huan, *ACS Nano* **2016**, *10*, 6623.
[119] N. Wang, L. Cheng, R. Ge, S. Zhang, Y. Miao, W. Zou, C. Yi, Y. Sun, Y. Cao, R. Yang, *Nat. Photonics* **2016**, *10*, 699.
[120] J. Song, J. Li, X. Li, L. Xu, Y. Dong, H. Zeng, *Adv. Mater.* **2015**, *27*, 7162.

[121] J. Li, L. Xu, T. Wang, J. Song, J. Chen, J. Xue, Y. Dong, B. Cai, Q. Shan, B. Han, H. Zeng, *Adv. Mater.* **2017**, *29*, 1603885.
[122] X. Gong, O. Voznyy, A. Jain, W. Liu, R. Sabatini, Z. Piontkowski, G. Walters, G. Bappi, S. Nokhrin, O. Bushuyev, *Nat. Mater.* **2018**, *17*, 550.
[123] M. K. Gangishetty, S. Hou, Q. Quan, D. N. Congreve, *Adv. Mater.* **2018**, *30*, 1706226.
[124] a) M. D. Smith, B. L. Watson, R. H. Dauskardt, H. I. Karunadasa, *Chem. Mater.* **2017**, *29*, 7083; b) L. Mao, Y. Wu, C. C. Stoumpos, B. Traore, C. Katan, J. Even, M. R. Wasielewski, M. G. Kanatzidis, *J. Am. Chem. Soc.* **2017**, *139*, 11956; c) L. Mao, Y. Wu, C. C. Stoumpos, M. R. Wasielewski, M. G. Kanatzidis, *J. Am. Chem. Soc.* **2017**, *139*, 5210.
[125] M. D. Smith, H. I. Karunadasa, *Acc. Chem. Res.* **2018**, *51*, 619.
[126] E. R. Dohner, E. T. Hoke, H. I. Karunadasa, *J. Am. Chem. Soc.* **2014**, *136*, 1718.
[127] Z. Yuan, C. Zhou, Y. Tian, Y. Shu, J. Messier, J. C. Wang, L. J. Van De Burgt, K. Kountouriotis, Y. Xin, E. Holt, *Nat. Commun.* **2017**, *8*, 14051.
[128] N. Arora, M. I. Dar, A. Hinderhofer, N. Pellet, F. Schreiber, S. M. Zakeeruddin, M. Grätzel, *Science* **2017**, *358*, 768.
[129] H. Aziz, Z. D. Popovic, N.-X. Hu, A.-M. Hor, G. Xu, *Science* **1999**, *283*, 1900.
[130] D. Bryant, N. Aristidou, S. Pont, I. Sanchez-Molina, T. Chotchunangatchaval, S. Wheeler, J. R. Durrant, S. A. Haque, *Energy Environ. Sci.* **2016**, *9*, 1655.
[131] H. Tsai, W. Nie, J.-C. Blancon, C. C. Stoumpos, R. Asadpour, B. Harutyunyan, A. J. Neukirch, R. Verduzco, J. J. Crochet, S. Tretiak, *Nature* **2016**, *536*, 312.
[132] X. Li, M. I. Dar, C. Yi, J. Luo, M. Tschumi, S. M. Zakeeruddin, M. K. Nazeeruddin, H. Han, M. Grätzel, *Nat. Chem.* **2015**, *7*, 703.
[133] W. Xiang, Q. Chen, Y. Wang, M. Liu, F. Huang, T. Bu, T. Wang, Y.-B. Cheng, X. Gong, J. Zhong, *J. Mater. Chem. A* **2017**, *5*, 5486.
[134] J.-W. Lee, H.-S. Kim, N.-G. Park, *Acc. Chem. Res.* **2016**, *49*, 311.
[135] J. C. Yu, D. W. Kim, D. B. Kim, E. D. Jung, J. H. Park, A. Y. Lee, B. R. Lee, D. Di Nuzzo, R. H. Friend, M. H. Song, *Adv. Mater.* **2016**, *28*, 6906.
[136] B. T. Diroll, G. Nedelcu, M. V. Kovalenko, R. D. Schaller, *Adv. Funct. Mater.* **2017**, *27*, 1606750.
[137] X. Yuan, X. Hou, J. Li, C. Qu, W. Zhang, J. Zhao, H Li, *Phys. Chem. Chem. Phys.* **2017**, *19*, 8934.
[138] H. Yuan, E. Debroye, K. Janssen, H. Naiki, C. Steuwe, G. Lu, M. l. Moris, E. Orgiu, H. Uji-i, F. De Schryver, *J. Phys. Chem. Lett.* **2016**, *7*, 561.
[139] N. Aristidou, C. Eames, I. Sanchez-Molina, X. Bu, J. Kosco, M. S. Islam, S. A. Haque, *Nat. Commun.* **2017**, *8*, 15218.
[140] S. J. Yoon, M. Kuno, P. V. Kamat, *ACS Energy Lett.* **2017**, *2*, 1507.
[141] H. Back, G. Kim, J. Kim, J. Kong, T. K. Kim, H. Kang, H. Kim, J. Lee, S. Lee, K. Lee, *Energy Environ. Sci.* **2016**, *9*, 1258.
[142] L. Zhao, R. A. Kerner, Z. Xiao, Y. L. Lin, K. M. Lee, J. Schwartz, B. P. Rand, *ACS Energy Lett.* **2016**, *1*, 595.
[143] A. Guerrero, J. You, C. Aranda, Y. S. Kang, G. Garcia-Belmonte, H. Zhou, J. Bisquert, Y. Yang, *ACS Nano* **2016**, *10*, 218.
[144] Y. Kato, L. K. Ono, M. V. Lee, S. Wang, S. R. Raga, Y. Qi, *Adv. Mater. Interfaces* **2015**, *2*, 1500195.
[145] K. Domanski, J.-P. Correa-Baena, N. Mine, M. K. Nazeeruddin, A. Abate, M. Saliba, W. Tress, A. Hagfeldt, M. Grätzel, *ACS Nano* **2016**, *10*, 6306.
[146] Y. Ling, Y. Tian, X. Wang, J. C. Wang, J. M. Knox, F. Perez-Orive, Y. Du, L. Tan, K. Hanson, B. Ma, *Adv. Mater.* **2016**, *28*, 8983.
[147] L. Zhao, Y.-W. Yeh, N. L. Tran, F. Wu, Z. Xiao, R. A. Kerner, Y. L. Lin, G. D. Scholes, N. Yao, B. P. Rand, *ACS Nano* **2017**, *11*, 3957.
[148] D. Liang, Y. Peng, Y. Fu, M. J. Shearer, J. Zhang, J. Zhai, Y. Zhang, R. J. Hamers, T. L. Andrew, S. Jin, *ACS Nano* **2016**, *10*, 6897.
[149] Z. Guo, X. Wu, T. Zhu, X. Zhu, L. Huang, *ACS Nano* **2016**, *10*, 9992.
[150] J. Liu, J. Leng, K. Wu, J. Zhang, S. Jin, *J. Am. Chem. Soc.* **2017**, *139*, 1432.